acid:polyribocytidylic acid (poly I:poly C) (Okamoto et al., 1999). The secretion of constitutive IFN-β from the stable transformants was apparently unpolarized. Meanwhile, intriguingly, IFN-β transiently expressed by gene transfection or induced by poly I:poly C was predominantly secreted from the cell membrane side to which the transfection or the induction was carried out. In this report, we have reconfirmed the secretion mode of IFN-β in epithelial Madin–Darby canine kidney (MDCK) cells and investigated the subcellular localization of the cytokine using GFP-tagged IFN-β under confocal laser scanning microscopy (CLSM). Our results suggested that IFNs expressed stably and transiently are transported via different post-TGN vesicles. This is the first report that the same secretory protein, at least as far as IFN is concerned, can be sorted to the apical or basolateral membrane side depending on the gene expression strategy, which deems to be regulated at the post-TGN stages.

MATERIALS AND METHODS

Cell lines

The MDCK cells (type I; ATCC-CCL-34), obtained from the American Type Culture Collection (Rockville, MD), were grown in Dulbecco's modified Eagle's medium (DMEM) (Nissui Pharmaceutical Co., Tokyo, Japan) supplemented with 10% fetal bovine serum (FBS), 1% nonessential amino acids, 100 U/ml penicillin, 100 μg/ml streptomycin, and L-glutamine (Gibco-Invitrogen Co., Carlsbad, CA). Mouse L and human FL cells, used for IFN bioassay, have been described previously (Okamoto et al., 1999).

Plasmid construction

The human IFN-β (HuIFN-β) and mouse IFN-β (MuIFN-β) expression plasmids, dubbed pCMV-HuIFNβ and pCMV-MuIFNβ, respectively, have been described previously (Kawabata et al., 1997; Nakanishi et al., 2002). To construct a human IFNβ–GFP fusion protein (HuIFNβ–GFP) expression vector, a fragment containing the full coding sequence of HuIFN-β was amplified by polymerase chain reaction (PCR) with the 5′ forward primer (5′-GACCCAAGCTTGGTACCGA-3′) and the 3′ reverse primer (5′-TGCTGAATTCGTTTCG-GAGGTAACGTGTAA-3′) from pCMV-HuIFNβ, followed by digestion with HindIII and EcoRI. The PCR fragment, in which the stop codon was converted to a codon for glutamic acid (Glu or E), was ligated into the HindIII-EcoRI site of the multiple cloning site of pEGFP-N1 (Clontech, Palo Alto, CA), having beforehand been undergone deletion of a sequence between the PstI and BamHI sites, to in-frame conjugate HuIFN-β to the N-terminus of GFP via an 8-amino acid spacer (EFDPPVAT). The resultant plasmid was designated pCMV-HuIFNβ–GFP, encoding a chimeric protein, HuIFNβ–GFP.

Transfection and establishment of stable lines

MDCK cells were seeded at 5×10^4 cells/cm^2 in 6-well plates, cultured for 24 h, and then transfected with expression vector DNA (3 μg/ml) complexed with 10 μg/ml cationic liposomes, Lipofectamine-2000 or Lipofectin (Gibco-Invitrogen Co.). To obtain stable transformants, the cell culture was split (1:20) and further continued in the presence of 1 mg/ml Geneticin (G418) (Gibco-Invitrogen Co.). Several G418-resistant single cell colonies were picked up and their GFP fluorescence examined by CLSM (see below) and, if necessary, their IFN production by bioassay (see below). Relatively strong positive sublines, named MDCK(HuIFNβ–GFP), MDCK(HuIFNβ), MDCK(MuIFNβ), and MDCK(GFP) for pCMV-HuIFNβ–GFP, pCMV-HuIFNβ, pCMV-MuIFNβ, and pEGFP-N1-derived transformants, respectively, were used in this work.

IFN bioassay

HuIFN-β and MuIFN-β activities in the supernatants of cell cultures were measured in FL and L cells, respectively, and expressed in antiviral units (U) as described previously (Watanabe and Kawade, 1987). If necessary, the type of the IFN activities were determined using specific neutralizing antibodies, mouse monoclonal antibody 8C3 (donation of YAMASA Shoyu Co., Ltd., Choshi, Japan) for HuIFN-β or rat monoclonal antibody 7F-D3 (Kawade and Watanabe, 1987) for MuIFN-β, as previously described (Okamoto et al., 1998).

Secretion polarity experiments

Cells ($1–2 \times 10^5$) were seeded onto Transwell filters (1 cm^2 culture area) (Costar, Cambridge, MA), and incubated for 5–7 days to obtain cell monolayers, which were monitored by measurement of the transepithelial electrical resistance (TER) of each cell sheet using a Millicell®-ERS meter (Millipore, Bedford, MA). The TER values of the monolayers of MDCK and the transformants used in this work were usually 800–1,300 (ohm × cm^2). For transient gene expression, the monolayers were washed twice with Opti-MEM (Gibco-Invitrogen Co.) and then challenged with IFN expression plasmids (3–5 μg/ml) complexed with Lipofectamine-2000 or Lipofectin (10 μg/ml) from the upper (apical transfection) or lower (basal transfection) compartment. After 4–6 h incubation, the cell sheets were washed twice, and the medium in both compartments was changed to regular growth medium. For stable expression, stable transformants were seeded and cultured similarly. The cell sheets were then washed twice, and the medium in both compartments was replaced with regular growth medium. In either expression experiment, the cell cultures were incubated for an additional 20 h and the culture fluids in both compartments were separately collected and subjected to IFN bioassay. In both experiments, 1 h after the last medium-change, a small amount of MuIFN-β or HuIFN-β (500–1,000 U) was added to the upper compartments as a permeability marker for HuIFN-β or MuIFN-β expression experiments, respectively. Each sample was thus assayed for expressed IFN activity and the marker IFNs in pertinent assay cell lines. In our bioassay, contamination by a small amount of MuIFN-β (lower than 1,000 U/ml) did not adversely affect the determination of the target HuIFN-β activity. No leakage of the marker IFN-β across the cell monolayer was observed in all the secretion polarity experiments performed (not shown).

Immunostaining and CLSM

Cells cultured on Transwell filters or coverslips were fixed with 4% paraformaldehyde in phosphate bufferred

saline (PBS) at room temperature for 20 min, permeabilized with 0.2% Triton-X 100-PBS for 20 min. If necessary, cell nuclei were stained by incubation with 0.5 μg/ml propidium iodide (PI) in 0.1 M NaCl–0.1 M Tris-HCl (pH 7.4) at room temperature for 20 min, following treatment with 15 μg/ml RNase A (Roche Diagnostics Co., Indianapolis, IN) at 37°C for 30 min and washing with PBS. Cells were, if necessary, further stained with specific primary and appropriate secondary antibodies (as mentioned below) in 1% BSA–1% Tween-20–PBS at room temperature for 1 h. Filters were cut out of the holders and mounted on coverslips. The cells on coverslips were immersed in 50% glycerol-2.5% DABCO (1,4-diazabicyclo-[2,2,2]octane) (Sigma-Aldrich Co., St. Louis, MO)-PBS. Emissions for optical x–y sections were collected using a confocal microscope (MRC-1024; BioRad, Hercules, CA) equipped with a Nikon Optiphot 2 microscope (Nikon, Tokyo, Japan) using 40× or 60× oil immersion objective. Collected x–y image segments were processed to obtain x–z images.

The following primary antibodies were used: mouse monoclonal antibodies against an ER resident protein, protein disulfide isomerase (PDI) (1D3) (Stressgen Biotechnologies Co., Victoria, Canada) (used at 1:200), a Golgi-associated protein, Golgi-58K (58K-9) (Sigma-Aldrich Co.) (at 1:50), and HuIFN-β (8C3) (YAMASA Shoyu Co.) (at 1:100), rat monoclonal antibody against MuIFN-β (6D-G8) (Kawade and Watanabe, 1987) (at 1:200) and rabbit polyclonal antibodies against a TGN-associated protein, furin convertase (Alexis Biochemicals, San Diego, CA) (at 1:100). The secondary antibodies were: Alexa Fluor 594-conjugated or Alexa Fluor 488-conjugated goat anti-mouse or anti-rabbit IgG (Molecular Probes, Inc., Eugene, OR) (at 1:100) and Alexa Fluor 546-conjugated goat anti-rat IgG (Molecular Probes, Inc.) (at 1:100) in 1% BSA–PBS.

Intracellular localization of HuIFNβ–GFP

Cells (1×10^5) were cultured on Transwell filters for 5 days. In the transient gene expression experiments, cells were transfected with pCMV-HuIFNβ–GFP from the apical or basal compartments and incubated for 10 h. Cells were fixed and permeabilized. For nucleus-staining, if necessary, the cells were further treated with RNase A, and then incubated with PI. To prevent or reduce ER-to-TGN and post-TGN transports and secretion processes, cells were treated with 5 μg/ml brefeldin A (BFA) (Sigma-Aldrich Co.) at 37°C for 30 min (Lippincott-Schwartz et al., 1991) or incubated in 10 mM HEPES-containing DMEM at 20°C for 2 h (Wacker et al., 1997) before cell fixation. For organelle immunostaining, cells were treated with corresponding antibodies mentioned above after cell fixation and permeabilization.

Cellular localization of stably and/or transiently expressed IFN-β

MDCK(HuIFNβ–GFP) or parental MDCK cells were grown on coverslips for 1 day. The former cells were transfected with pCMV-MuIFNβ, and the latters co-transfected with pCMV-HuIFNβ–GFP and pCMV-MuIFNβ. Eight hours after transfection, the cells were incubated with 10 μg/ml cycloheximide (CHX) (Biomol Research Labs, Inc., Plymouth Meeting, PA) and 10 mM HEPES-containing DMEM for 2 h at 20°C. The cells on coverslips were then transferred to 10 μg/ml CHX-containing DMEM at 37°C, and incubated for 30 min. These procedures enabled us to examine the gene products accumulated during the treatment without any overlap by newly synthesized gene products, at least for 30 min after temperature up-shift. Cells were fixed, permeabilized, and then stained with primary rat anti-MuIFN-β antibody (6D-G8) and secondary Alexa Fluor 546-conjugated goat anti-rat IgG, before carrying out the CLSM studies. Image analysis for co-localization (Manders et al., 1993) was performed using the software, Image-Pro Plus ver. 4.5 (Media Cybernetics, Inc., Silver Spring, MD). From scatter-plots of the pixel fluorogram, co-localization coefficients, M_1 (contribution of green) and M_2 (contribution of red), were computed for intensity ranges defined by arbitrary area of interest (AOI) along the diagonal line of each scatter-plot based on the following equations:

$$M_1 = \frac{\sum_i S1_{i,\mathrm{coloc}}}{\sum_i S1_i} \quad \text{and} \quad M_2 = \frac{\sum_i S2_{i,\mathrm{coloc}}}{\sum_i S2_i}$$

where $S1_i$ or $S2_i$ is signal intensity of ith pixel in the first (green) or second (red) channel, respectively. $S1_{i,\mathrm{coloc}} = S1_i$, if $S2_i$ is within thresholds defined by AOI, $S1_{i,\mathrm{coloc}} = 0$, if $S2_i$ is out side the threshold levels. $S2_{i,\mathrm{coloc}} = S2_i$, if $S1_i$ is within thresholds, $S2_{i,\mathrm{coloc}} = 0$, if $S1_i$ is outside the AOI.

RESULTS

As shown in Figure 1, the secretion profile of IFN-β exogenously expressed in epithelial MDCK was essentially the same as that in mouse epithelial Pam-T cells (Nakanishi et al., 2002). Stably expressed human or mouse IFN-β was almost equally secreted from both the apical and basal cell membrane sides, while transiently expressed IFN-β was predominantly secreted to the upper or lower compartment from which the gene transfection was performed.

The expression plasmid for GFP-tagged HuIFN-β was generated to trace the intracellular routes of IFN-β molecules. The chimeric HuIFNβ–GFP exhibited antiviral activity and susceptibility to the specific antibody against HuIFN-β (not shown). The secretion profiles of HuIFNβ–GFP in MDCK cells was essentially the same as HuIFN-β or MuIFN-β (Fig. 2B), indicating that GFP-tagging does not affect the secretion polarity of IFN-β.

Next, HuIFNβ–GFP expressed in MDCK cells was immunostained with the specific anti-HuIFN-β antibody (8C3) and analyzed by confocal microscopy. As shown in Figure 2A, a–c, the cellular signals of GFP and HuIFN-β coincided (Fig. 2A, a–c) with a similar distribution pattern of HuIFN-β signals in the cells harboring pCMV-HuIFNβ, which showed cytoplasmic dotted aggregation (Fig. 2A, e), different from the pattern of GFP in the cells harboring pEGFP-N1, which showed homogeneous distribution of GFP throughout the cells (Fig. 2A, g). These results suggest that the fusion protein is a hybrid of intact IFN-β and intact GFP in the cell.

Figure 3 shows the intracellular localization of GFP in MDCK(GFP) monolayers (A), HuIFNβ–GFP in

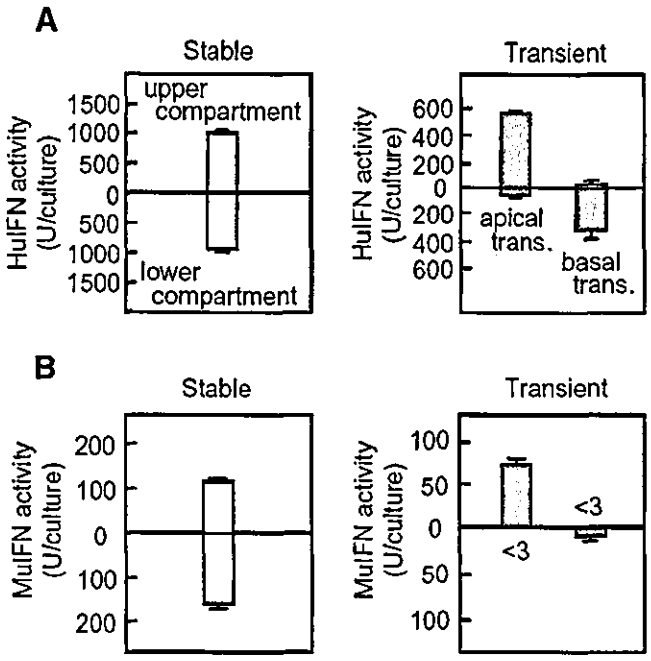

Fig. 1. Secretion polarity of IFN-β stably and transiently expressed in MDCK cells. Cells were grown in Transwell plates to form monolayers. A: Secretion profile of human IFN-β (HuIFN-β) expressed in stable transformants (left part) and transiently in MDCK cells (right part). B: Secretion profile of mouse IFN-β (MuIFN-β) expressed stably (left part) and transiently (right part). Transient expression was performed by two types of transfection mode, apical and basal transfection. The scales above and below the null line indicate the IFN activities in the upper and lower compartments, respectively. Each value represents the mean ± SD (n = 3).

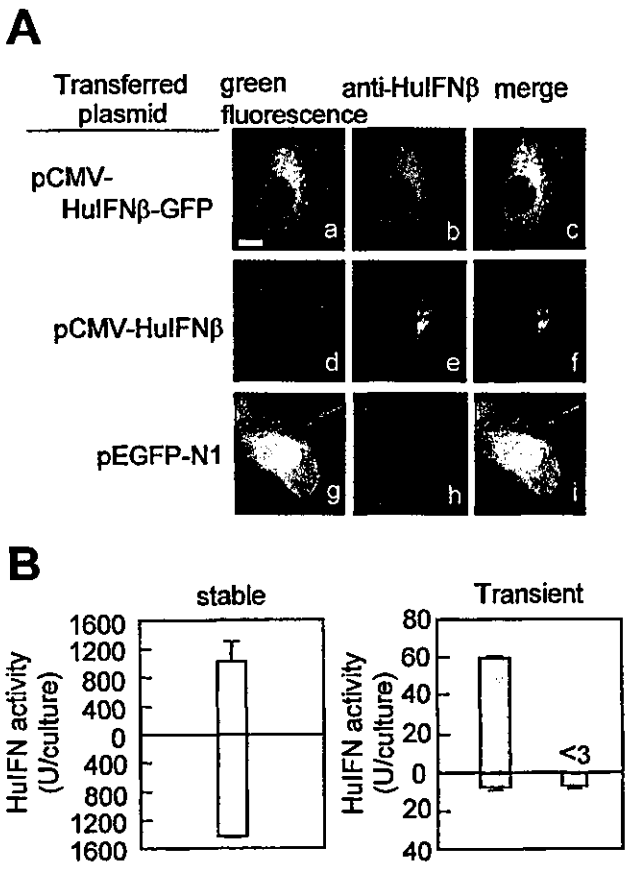

Fig. 2. Visualization and secretion polarity of human IFNβ-green fluorescent protein (GFP). A: Stable MDCK transformants harboring pCMV-HuIFNβ-GFP (a–c), pCMV-HuIFNβ (d–f), or pEGFP-N1 (g–i), cultured on coverslips, were fixed, permeabilized and stained with 8C3 antibody against HuIFN-β and secondary Alexa Fluor 594-conjugated goat anti-mouse IgG, followed by confocal imaging of green fluorescence (a, d, g), red color (b, e, h), and those over-lay (c, f, i). All images are of the same magnification; the white scale bar in part a represents 10 μm. B: Left graph shows the secretion of IFN activity from the stable transformants producing human IFNβ-GFP. Right graph shows the secretion from the cells following transfection of pCMV-HuIFNβ-GFP from the apical (left gray bar) or basal (right gray bar) side. Each value represents the mean ± SD of three separated experiments.

MDCK(HuIFNβ–GFP) monolayers (B), and HuIFNβ–GFP in parental MDCK monolayers transiently expressed with pCMV-HuIFNβ–GFP by transfection from apical (C) or basal side (D), under BFA treatment. A fungal metabolite BFA, a potent inhibitor of vesicle formation from the Golgi apparatus, was used to increase the number of visible cells expressing HuIFNβ–GFP and enhance the fluorescence intensity in the cells. The GFP of MDCK(GFP) distributed throughout the cytoplasm (Fig. 3A). Meanwhile, the signals derived from HuIFNβ–GFP were mainly localized at the upper side of the nuclei regardless of stable or transient expression, and regardless of the direction of gene delivery, apical or basal transfection (Fig. 3B–D).

To examine the subcellular localization of HuIFNβ–GFP, initially we stained MDCK cells grown on filters with antibodies against PDI (Bassnett and Mataic, 1997), Golgi-58K (Bloom and Brashear, 1989), and furin convertase (Jou et al., 2000) as specific ones for subcellular organelles, ER, Golgi, and TGN, respectively (Fig. 4). Next, we investigated the spatial relationship of the cellular localization of stably (Fig. 5A) or transiently (Fig. 5B) expressed HuIFNβ–GFP to the subcellular organelles, ER (a–c and m–o), Golgi (d–f and p–r) and TGN (g–i and s–u), which convey secretory proteins, in MDCK cell monolayers with or without BFA block and 20°C treatment. BFA is known to inhibit ER-Golgi translocation of newly synthesized secretory proteins and subsequently cause the accumulation of the proteins in ER (Lippincott-Schwartz et al., 1991). Temperature treatment at 20°C also attenuates the translocation of secretory proteins as well as protein biosynthesis (Wacker et al., 1997). Consequently, stably and transiently expressed HuIFNβ–GFP molecules were seen partly in the area of Golgi and substantially in the area of Golgi and/or TGN apparatuses. These results suggest that stably and transiently expressed HuIFNβ–GFPs were transported through common pathway(s) from ER to Golgi/TGN.

To elucidate whether there is a difference in the transport of IFN-β after the TGN between stable expression and transient expression, initially we confirmed the secretion polarity of MuIFN-β expressed in stable MDCK(HuIFNβ–GFP) cells following transfection with pCMV-MuIFNβ. As shown in Figure 6, the transiently expressed MuIFN-β was predominantly

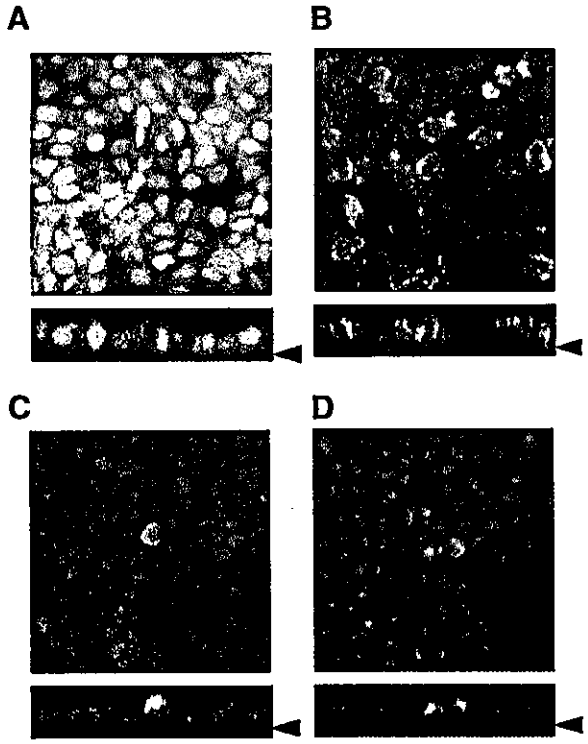

Fig. 3. Intracellular localization of GFP and human IFNβ–GFP expressed in MDCK. Stable MDCK(GFP) (A) and MDCK(HuIFNβ–GFP) (B) cells were cultured on Transwell for 5 days. Parental MDCK cells, being similarly cultured, were transfected with pCMV-HuIFNβ–GFP from the apical (C) or basal (D) side, and incubated for 10 h. All cells except for MDCK(GFP) were treated with BFA for 30 min prior fixation, and then subjected to PI treatment. Typical confocal x–y field images are shown together with a x–z section at the bottom. The red color of PI indicates nuclei. Arrowheads denote the position of filters.

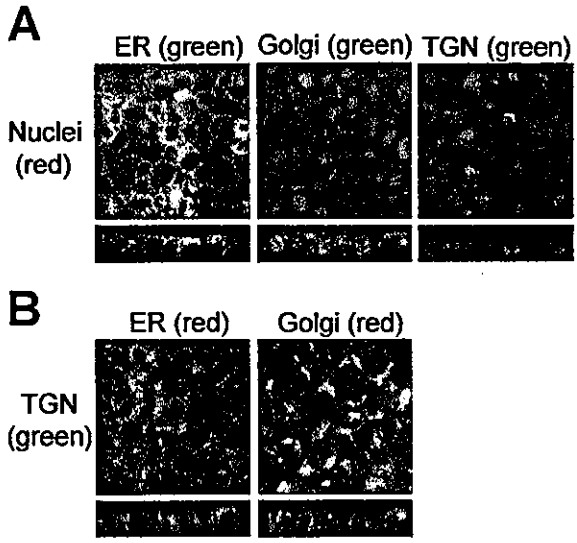

Fig. 4. Immunostaining of endoplasmic reticulum (ER), Golgi, and TGN in MDCK cells. A: MDCK monolayers, cultured on Transwell as in Figure 2, were stained with primary antibodies against PDI for ER, Golgi-58K for Golgi or furin convertase for TGN, and then with appropriate secondary Alexa Fluor 488 (green)-conjugated antibodies, followed by treatment with PI for cell nuclei (red). B: MDCK monolayers were stained with double primary antibodies against furin convertase (for TGN) and PDI (for ER) or Golgi-58K (for Golgi), and then with appropriate double secondary antibodies conjugated with Alexa Fluor 594 (red) and Alexa Fluor 488 (green). Top and bottom parts show the x–y and x–z fields of confocal microscopy, respectively.

secreted to the side from which the transfection was carried out, while the stable expression of HuIFNβ–GFP remained unpolarized.

Next, we settled the conditions of temperature and CHX treatment that reduce post-TGN transport and inhibit de novo protein synthesis, respectively. Such conditions enable to follow IFNs in the Golgi apparatus without being disturbed by newly synthesized ones. MDCK(HuIFNβ–GFP) cells were treated with 0, 10, 20 μg/ml CHX for 2 or 4 h at 20 or 37°C and then subcellular HuIFNβ–GFP was observed by using confocal microscopy. As shown in Figure 7A, treatment with 10 μg/ml CHX for 2 h at 20°C caused efficient accumulation of HuIFNβ–GFP in MDCK(HuIFNβ–GFP) cells. When cells were treated with 10 μg/ml CHX for 2 h at 37°C, subcellular IFNs were not observed (Fig. 7B, h) indicating that 10 μg/ml CHX is enough to completely inhibit the synthesis of IFN. When discharged from the restriction, the cells displayed IFN secretion with a retardation (about 30 min) compared with control cells (Fig. 7C).

As the signals were very weak in the side view (x–z image) of cell monolayers, we carried out two types of experiments with cells grown on coverslips: (1) transient expression of MuIFN-β in stable MDCK(HuIFNβ–GFP) cells and (2) transient co-expression of MuIFN-β and HuIFNβ–GFP in parental MDCK cells.

In each case, both types of IFN molecules accumulated and apparently mingled/co-localized at TGN by CHX treatment at 20°C as shown by a merging of red and green to yield a orange–yellow distribution (Fig. 8A,B, time 0). The accumulated IFNs were released in a time-dependent fashion and dispersed to the peripheral cytoplasm as small vesicles, following a temperature shift to 37°C. In experiment (1), significant amounts of MuIFN-β and HuIFNβ–GFP appeared to be dispensed to distinct small vesicles which contained each type of molecules (Fig. 8A, 30 min). In experiment (2), both types of molecules were co-distributed into small post-Golgi vesicles (Fig. 8B, 30 min); indeed, the merged images in Fig. 8B revealed orange-yellow punctuate distribution still present at 30 min after up-shift of temperature (notice the arrowheads in part f), but such distribution was not seen in Figure 8A, part b. The respective scatter-plots (Fig. 8A,B, lower parts) deduced from the merged images (Fig. 8A,B, upper parts) further confirmed the significant degree of the fluorescence spatial-co-localization of these two probes. The relative values of co-localization coefficients, M_1 (contribution of green) and M_2 (contribution of red) (Fig. 8A,B, at the bottom of the parts), are consistent with this situation.

DISCUSSION

We have investigated the secretion mode of IFN-β exogenously expressed in MDCK cell monolayers and found that the mode differs between stable expression

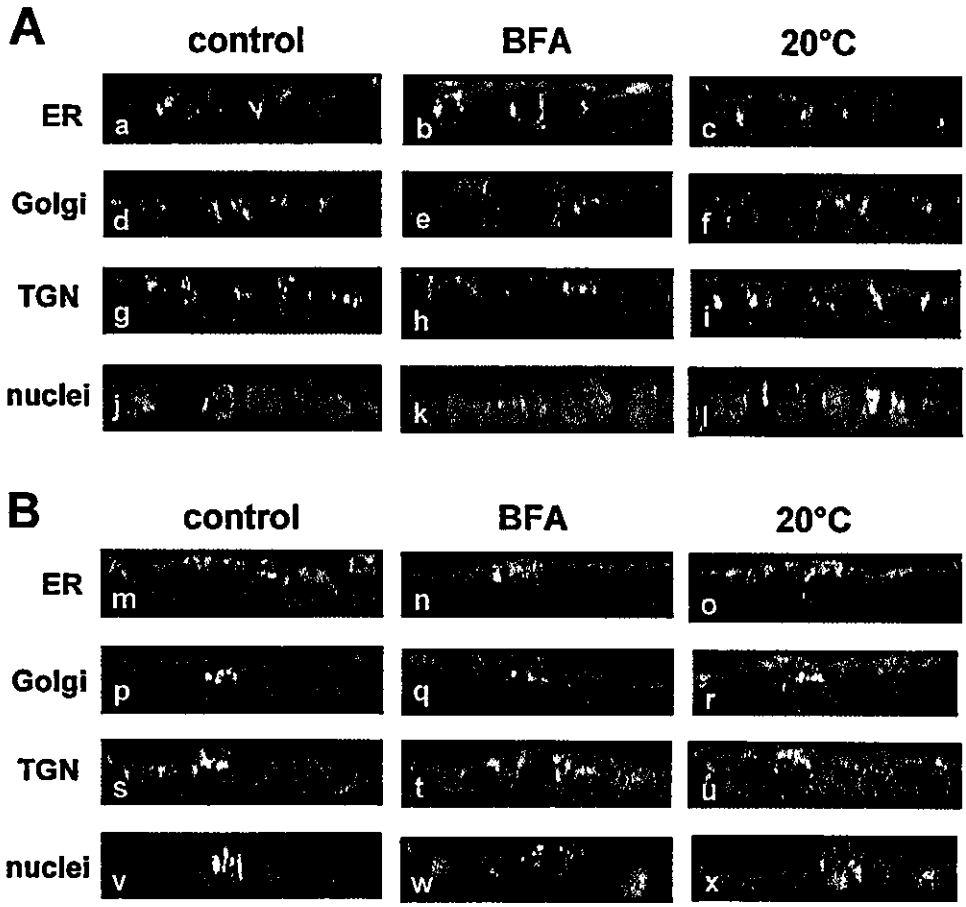

Fig. 5. Relative localization of human IFNβ–GFP expressed in MDCK monolayers to various organelles. MDCK(HuIFNβ–GFP) (**A**) and parental MDCK (**B**) monolayers were grown as in Figure 2. The latter monolayers were apically transfected with pCMV-HuIFNβ–GFP and incubated for 10 h. Either monolayer was treated with 20°C for 2 h or with BFA (5 μg/ml) for 30 min just prior fixation, followed by staining with the ER- (**a–c, m–o**), Golgi- (**d–f, p–r**), or TGN-specific antibodies (**g–i, s–u**) and appropriate secondary antibodies, or alternatively with PI for nuclei (**j–l, v–x**). In control experiments, no 20°C treatment or BFA treatment was carried out. Typical x–z sections of the confocal images are shown.

from transformants and transient expression from parental cells transfected with expression vectors in harmony with the previous reports with other epithelial cells (Kawabata et al., 1997; Nakanishi et al., 2002); in stable expression, IFN was almost equally secreted to the apical and basal cell membrane sides. In transient expression, IFN was predominantly secreted from the cell membrane side to which the transfection was carried out. Thus, it is unlikely that *N*-glycans of IFN-β was the dominant sorting signals in our experiments, although it has been proposed that *N*-glycans act as apical sorting signals in many secretory glycoproteins (Scheiffele et al., 1995; Kuhn et al., 2000).

The phenomenon of transfection-side dependent secretion of exogenous gene products was not restricted to IFN-β and was observed on IFN-γ and TNF-α as well (data not shown). We had previously demonstrated also that endogenous IFN expression in polarized epithelial cell lines after treatment with an IFN inducer, poly I:poly C, showed stimulation side dependent asymmetrical secretion (Okamoto et al., 1999). Thus, the phenomenon was not specific for exogenous gene expression and not for IFN-β or type I IFN. In addition, it was not dependent on the modality of gene delivery as similar results were obtained for gene delivery with fusogenic HVJ liposomes (Saeki et al., 1997) (not shown). Intriguingly, however, this phenomenon was not observed in all types of epithelial cells, since the transient secretion of IFN in swine LLC-PK$_1$ and

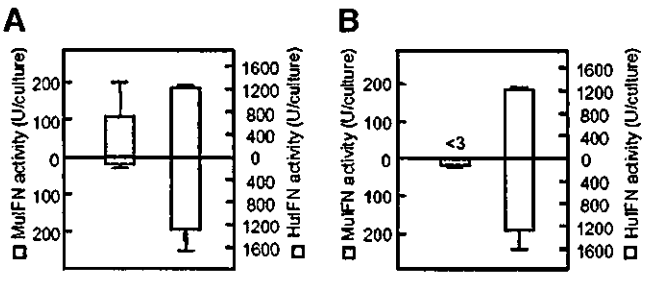

Fig. 6. Secretion of IFN activities from MDCK(HuIFNβ–GFP) cells following transfection of the mouse IFN-β (*MuIFN-β*) gene. pCMV-MuIFNβ was applied to the apical side (**A**) or to the basal side (**B**). Shaded and open bars indicate mouse and human IFN activities, respectively. The values represent the means of three determinations with SD.

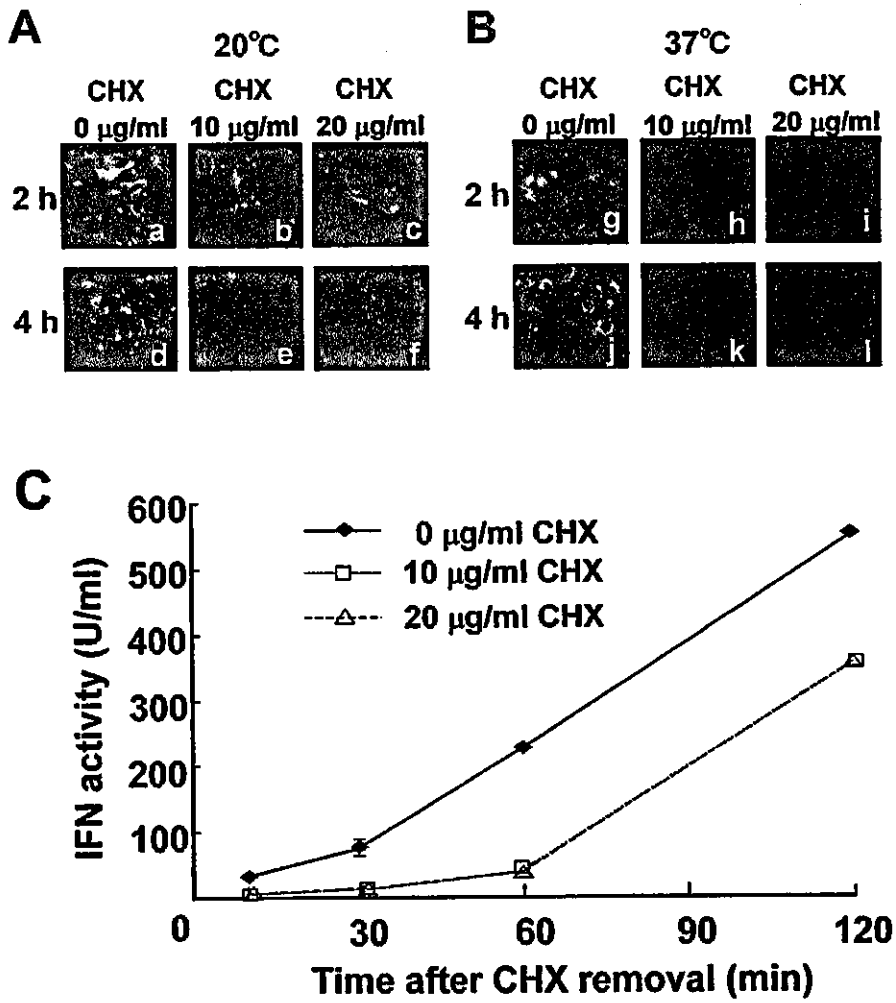

Fig. 7. Effects of cycloheximide (CHX) and temperature on cellular processing and secretion of HuIFNβ–GFP. Stable MDCK(HuIFNβ–GFP) cells cultured on coverslips were treated for 2 or 4 h with 0, 10, or 20 μg/ml CHX at 20°C (A) or 37°C (B), followed by fixation and confocal microscopy. In parallel, secretion of the IFN activity from MDCK(HuIFNβ–GFP) (C) was examined; after treatment with 0, 10, or 20 μg/ml CHX for 2 h, cells were incubated in regular medium without CHX at 37°C. During the incubation, aliquots of culture fluids were picked up at indicated time points and assayed for antiviral activity. Each value represents the mean ± SD of three separated experiments. [Color figure can be viewed in the online issue, which is available at www.interscience.wiley.com.]

another type of MDCK (type II) cell monolayers was non-polarized (unpublished results). The reason for this discrepancy is unclear at present.

To directly visualize subcellular IFN during secretion, we produced an expression vector for HuIFN-β coupled to GFP, HuIFNβ–GFP. The fusion protein consists of full length HuIFN-β and enhanced GFP, which are conjugated via an 8-amino acid spacer. This size of spacer seems not to disrupt the intact folding of each protein (Wahlfors et al., 2001). Our observations imply that there is no difference in the transport routes of HuIFNβ–GFP from ER to TGN among stable expression, and apical or basal transient expression in MDCK cell monolayers.

We further investigated the post-TGN transport of IFN-β in MDCK cells by co-expression of MuIFN-β and HuIFNβ–GFP and unexpectedly found that the post-TGN transport seemed to differ between transient and stable expression (Fig. 8). MuIFN-β, and HuIFN-βs are, although discriminated by specific antibodies, structurally homologous and expected to obey the same transporting mechanisms. When the expression vectors for MuIFN-β and HuIFNβ–GFP were co-transfected onto MDCK cells, both gene products co-localized even in post-TGN vesicles. Meanwhile, when pCMV-MuIFN-β was transiently expressed in MDCK(HuIFNβ–GFP) cells, MuIFN-β showed different localization from HuIFNβ–GFP. In other words, taken together, there are at least two distinct post-TGN transport routes for secretory proteins, one for stably expressed proteins and the other for transiently expressed ones. This difference presumably reflects the transfection side-dependent secretion polarity of the cytokine in polarized epithelial cells such as MDCK and Pam-T cells. Post-TGN steps seem to be critical for vectorial apical or basolateral transport, as reported by others (Keller et al., 2001) with apical or basorateral sorting of membrane proteins, although the mechanisms are not fully understood.

The transfection side-dependent secretion profile may be due to transient disruption of intracellular

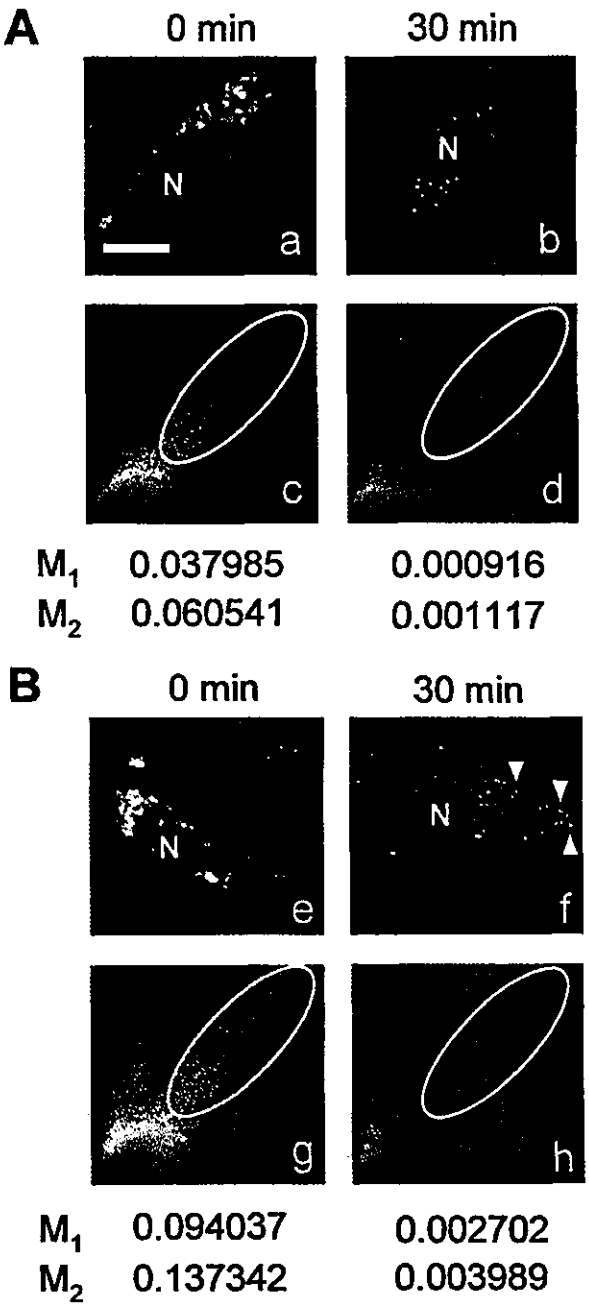

Fig. 8. Post-TGN localization of MuIFN-β and human IFNβ–GFP expressed in MDCK cells. A: Stable MDCK(HuIFNβ–GFP) cells were transfected with pCMV-MuIFNβ. B: Parental MDCK cells were co-transfected with pCMV-HuIFNβ–GFP and pCMV-MuIFNβ. After transfection, cells were incubated for 8 h and then subjected to 20°C-treatment for 2 h. Thereafter, cells were warmed to 37°C (time 0) (**a**, **e**) and incubated for 30 min (**b**, **f**), followed by fixation and staining with rat anti-MuIFN-β IgG (6D-G8) and Alexa Fluor 546-conjugated goat anti-rat IgG for confocal microscopy. Typical merged images are shown. N indicates the nucleus. Notice that several orange–yellow spots are pointed by white arrowheads in part f. Scatter-plots of the pixel fluorogram (ordinate for green; abscissa for red) of the merged images are shown in the respective lower parts (**c**, **d**, **g**, **h**), in which the AOI region selected is surrounded by white line, together with co-localization coefficients, M_1 (contribution of green) and M_2 (contribution of red) at the bottom. The scale bar in part a represents 10 μm.

membrane trafficking induced by cationic liposome-mediated gene transfection. This is, however, unlikely because the stable secretion mode was not affected by such transfection either from apical or basal side (data not shown), agreeing with previous observations involving Pam-T cells (Nakanishi et al., 2002).

The different transcription fields of transient and stable gene expression in the nucleus may contribute to the different secretion modes. In stable line, the exogenous IFN genes are integrated into the host cell genomes and expressed as if inherent genes. Meanwhile, in transient gene expression, the exogenous IFN genes, imported into the nuclei, are transcribed at the nuclear matrices off the chromosomes. According to the recent dynamic mosaic model for transcription (Wei et al., 1998), the transcription sites are compartmented into multiple regions in the nucleus. After transcription in the compartments, the resultant transcripts, not diffusing but being confined to some "micro-carriages," are conveyed via some defined "tracks" to the extranuclear cytoplasm, where the following events, including translation and posttranslational modification, take place while they are confined to the ER-Golgi system; the products are sorted to defined cell surfaces, presumably via the cytoskeletal apparatus. In stable expression, exogenous genes are integrated multiply (Tseng et al., 1997) and randomly in the genome and the active transcription sites for their promoter will be scattered at random throughout the nuclear matrix. Thus, the posttranscriptional processes are trafficked to various directions and the overall secretion is apparently unpolarized. In this ad-hoc hypothesis, positional information of transcription in the nucleus may somehow be reflected in the sorting direction of the gene products.

At any rate, in the present study, we have suggested that stably and transiently expressed IFNs, even though co-localized at TGN, are transported presumably through apparently discriminated post-TGN routes depending on the gene transfection-side in some polarized epithelial cells. Our approach will provide a novel insight into the sorting mechanism of secretory proteins in epithelial cells.

LITERATURE CITED

Bassnett S, Mataic D. 1997. Chromatin degradation in differentiating fiber cells of the eye lens. J Cell Biol 138:37–49.

Bloom GS, Brashear TA. 1989. A novel 58-kDa protein associates with the Golgi apparatus and microtubules. J Biol Chem 264:16083–16092.

Griffiths G, Simons K. 1986. The trans Golgi network: Sorting at the exit site of the Golgi complex. Science 234:438–443.

Jou TS, Leung SM, Fung LM, Ruiz WG, Nelson WJ, Apodaca G. 2000. Selective alterations in biosynthetic and endocytic protein traffic in Madin–Darby canine kidney epithelial cells expressing mutants of the small GTPase Rac1. Mol Biol Cell 11:287–304.

Kawabata K, Kondo M, Watanabe Y, Takakura Y, Hashida M. 1997. Non-polarized secretion of mouse interferon-β from gene-transferred human intestinal Caco-2 cells. Pharm Res 14:483–485.

Kawade Y, Watanabe Y. 1987. Characterization of rat monoclonal antibodies to mouse interferon-α and -β. In: Cantell K, Schellekens H, editors. The biology of the interferon system. Dordrecht: Martinus Nijhoff. pp 27–29.

Keller P, Simons K. 1997. Post-Golgi biosynthetic trafficking. J Cell Sci 110:3001–3009.

Keller P, Toomre D, Díaz E, White J, Simons K. 2001. Multicolour imaging of post-Golgi sorting and trafficking in live cells. Nat Cell Biol 3:140–149.

Kuhn U, Cohn DV, Gorr SU. 2000. Polarized secretion of the regulated secretory protein chromogranin A. Biochem Biophys Res Commun 270:631–636.

Lippincott-Schwartz J, Patterson GH. 2003. Development and use of fluorescent protein markers in living cells. Science 300:87–91.

Lippincott-Schwartz J, Yuan L, Tipper C, Amherdt M, Lelio Orci L, Klausner RD. 1991. Brefeldin A's effects on endosomes, lysosomes, and the TGN suggest a general mechanism for regulating organelle structure and membrane traffic. Cell 67:601–616.

Lippincott-Schwartz J, Roberts TH, Hirschberg K. 2000. Secretory protein trafficking and organelle dynamics in living cells. Annu Rev Cell Dev Biol 16:557–589.

Manders EMM, Verbeek FJ, Aten JA. 1993. Measurement of co-localization of objects in dual-colour confocal images. J Microsc 169:375–382.

Nakanishi K, Watanabe Y, Maruyama M, Yamashita F, Takakura Y, Hashida M. 2002. Secretion polarity of interferon-β in epithelial cell lines. Arch Biochem Biophys 402:201–207.

Okamoto S, Watanabe Y, Takakura Y, Hashida M. 1998. Cationic liposome-mediated efficient induction of type I interferons by a low dose of poly I:poly C in mouse cell lines. J Biochem 124:697–701.

Okamoto S, Nakanishi K, Watanabe Y, Yamashita F, Takakura Y, Hashida M. 1999. Stimulation side-dependent asymmetrical secretion of poly I:poly C-induced interferon-β from polarized epithelial cell lines. Biochem Biophys Res Commun 254:5–9.

Rodriguez-Boulan E, Nelson WJ. 1989. Morphogenesis of the polarized epithelial cell phenotype. Science 245:718–725.

Saeki Y, Matsumoto N, Nakano Y, Mori M, Awai K, Kaneda Y. 1997. Development and characterization of cationic liposomes conjugated with HVJ (Sendai virus): Reciprocal effect of cationic lipid for in vitro and in vivo gene transfer. Hum Gene Ther 8:2133–2141.

Scheiffele P, Peranen J, Simons K. 1995. *N*-glycans as apical sorting signals in epithelial cells. Nature 378:96–98.

Tseng W-C, Haselton FR, Giorgio TD. 1997. Transfection by cationic liposomes using simultaneous single cell measurements of plasmid delivery and transgene expression. J Biol Chem 272: 25641–25647.

Tsien RY. 1998. The green fluorescent protein. Annu Rev Biochem 67:509–544.

Wacker I, Kaether C, Kromer A, Migala A, Almers W, Gerdes HH. 1997. Microtubule-dependent transport of secretory vesicles visualized in real time with a GFP-tagged secretory protein. J Cell Sci 110:1453–1463.

Wahlfors J, Loimas S, Pasanen T, Hakkarainen T. 2001. Green fluorescent protein (GFP) fusion constructs in gene therapy research. Histochem Cell Biol 115:59–65.

Wandinger-Ness A, Bennett MK, Antony C, Simons K. 1990. Distinct transport vesicles mediate the delivery of plasma membrane proteins to the apical and basolateral domains of MDCK cells. J Cell Biol 111:987–1000.

Watanabe Y, Kawade Y. 1987. Induction, production, and purification of natural mouse IFN-α and -β. In: Clemens MJ, Morris AG, Gearing AJH, editors. Lymphokines and interferons: A practical approach. Oxford: IRL Press. pp 1–14.

Wei X, Samarabandu J, Devdhar RS, Siegel AJ, Acharya R, Berezney R. 1998. Segregation of transcription and replication sites into higher order domains. Science 281:1502–1505.

Available online at www.sciencedirect.com
SCIENCE DIRECT®
Biochemical and Biophysical Research Communications 321 (2004) 886–892
BBRC
www.elsevier.com/locate/ybbrc

Alteration of the timing of implantation by in vivo gene transfer: delay of implantation by suppression of nuclear factor κB activity and partial rescue by leukemia inhibitory factor

Hitomi Nakamura [a], Tadashi Kimura [a,*], Kazuhide Ogita [a], Shinsuke Koyama [a], Tomoko Tsujie [a], Tateki Tsutsui [a], Koichiro Shimoya [a], Masayasu Koyama [a], Yasufumi Kaneda [b], Yuji Murata [a]

[a] *Division of Obstetrics and Gynecology, Department of Specific Organ Regulation, Osaka University Graduate School of Medicine, 2-2, Yamadaoka, Suita, Osaka 5650871, Japan*
[b] *Division of Gene Therapy Science, Osaka University Graduate School of Medicine, 2-2, Yamadaoka, Suita, Osaka 5650871, Japan*

Received 11 June 2004
Available online 28 July 2004

Abstract

Nuclear factor κB (NF-κB) is activated in the murine endometrium during implantation period [Am. J. Reprod. Immunol. 51 (2004) 16]. Transient transfection of IκBα mutant (IκBαM) cDNA into the mouse uterine cavity using hemagglutinating virus of Japan envelope vector suppressed uterine NF-κB activity less than half of that observed in control on days 3.5 and 4.5 p.c. IκBαM cDNA transfection led to significant delay of implantation. After IκBαM cDNA transfection, LIF mRNA expression in the uterus was significantly suppressed on days 3.5 and 4.5 p.c. Co-transfection of LIF cDNA with IκBαM cDNA in the uterus partially rescued the delay of implantation induced by suppression of NF-κB activity. Taken together, these findings indicate that NF-κB activation determines the timing of the implantation, at least in part, via control of LIF expression.

Keywords: In vivo gene transfer; Mouse; Uterus; Implantation; Hemagglutinating virus of Japan envelope vector; Nuclear factor κB; IκBα; Leukemia inhibitory factor

During implantation, expression of various kinds of hormones, autacoids, cytokines, growth factors, and matrix substances has been reported in the uterus. These molecules are under strict temporal and spatial regulation of maternal hormones and probably fetus-derived substances. Because of this strict regulation, implantation can only occur within very short period, namely the implantation window, beginning on day 3.5 post coitus (p.c.; the morning when the vaginal plug is observed is taken as day 0.5 p.c.) in the rodent uterus [2]. Among the known regulatory factors, ovarian steroid hormones play crucial roles in determining the timing of the implantation window, because modulation of steroid hormones by ovariectomy and exogenous administration caused dormancy of implantation [3]. However, there is no proof that ovarian steroids directly regulate the molecules up-regulated at the implantation window, of which genes have no authentic steroid hormone responsive elements. We therefore speculate that a few multipotential transcription factors might regulate the transcription of various kinds of molecules that initiate the cascade of biochemical modification of the endometrium to open the implantation window.

Nuclear factor κB (NF-κB) is a transcription factor that is involved in many kinds of inflammatory and

Corresponding author. Fax: +81-6-6879-3359.
E-mail address: tadashi@gyne.med.osaka-u.ac.jp (T. Kimura).

0006-291X/$ - see front matter © 2004 Elsevier Inc. All rights reserved.
doi:10.1016/j.bbrc.2004.07.045

immune responses. Some genes whose expression is closely related to implantation, such as cyclooxygenase II (COX-2), leukemia inhibitory factor (LIF), and colony stimulating factor (CSF)-I, are under the transcriptional control, at least in part, of the NF-κB system [4]. It has been reported that exogenous estradiol treatment activates NF-κB [5] and that NF-κB is activated at the time of the implantation in the mouse and human uterus [1,6]. Based on these observations, we speculate that NF-κB may play crucial roles in determining the timing of implantation. However, previous gene targeting strategies for the NF-κB system did not yield any information about the function of NF-κB during the implantation period in the uterine endometrium [7–10]. To examine the function of activated NF-κB during the implantation period, we transiently transfected the inhibitory κBα mutant (IκBαM) cDNA, which lacks signal-dependent phosphorylation sites and cannot dissociate from NF-κB, into the mouse uterine cavity using HVJ-E vector system [11].

Materials and methods

Animals. Female ICR mice (SLC, Shizuoka, Japan) aged 8–10 weeks in estrus were bred with male ICR mice, and the morning when vaginal plugging was observed was designated as day 0.5 p.c., and the successfully bred female was separated from male. A time breeding procedure was employed to precisely control the time of insemination. All animal experiments were performed according to the appropriate guidelines for animal use approved by the Institutional Animal Care and Use Committee of Osaka University Graduate School of Medicine.

DNA preparation. IκBαM cDNA (BD Biosciences Clontech, CA, USA) was introduced into the pcDNA3 expression vector (cytomegalovirus promoter driven; Invitrogen, San Diego, CA) at the *Hin*dIII–*Bam*HI sites (pcDNA3-IκBαM). The cDNA of murine leukemia inhibitory factor (LIF) was distributed from RIKEN BRC DNA Bank (RDB 1484, http://www.rtc.riken.go.jp/cgi-bin/DNA/show.d.pl?keyword=1484&). The open reading frame of LIF cDNA was excised by *Hin*dIII–*Not*I and introduced into pcDNA3 plasmid (pcDNA3-LIF). Plasmid DNA was purified using a Qiagen column (Tokyo, Japan). Control gene transfers were performed using pcDNA3 and/or pcDNA-LacZ [11] plasmid DNA.

Preparation of HVJ-envelope vector. HVJ (hemagglutinating virus of Japan, also known as Sendai virus) was amplified as described previously [12]. Virus was inactivated by UV irradiation and inactivated virus suspension (10,000 hemagglutinating activity units (HAU)) was mixed with 800 μg (single transfection) or 1600 μg (co-transfection of two plasmids) of plasmid DNA. Trapping efficiency of the plasmid in HVJ envelope (HVJ-E) vector was approximately 15–20% [13]. Plasmid-incorporated HVJ-E vector was finally suspended in 250 μl of human tubal fluid (HTF) medium (Nippon Medical and Chemical Instrument, Osaka, Japan) as described previously [11].

In vivo gene transfer. Mice on day 1.5 p.c. were anesthetized and subjected to laparotomy to expose the uterus. Twenty-five microliters/horn of HVJ-E vector suspension was injected slowly into the uterine cavity using a 30-gauge needle, and the cervix was clamped for 10 min. Then the incision was closed to allow recovery of the mice.

Tissue sampling and analysis of implantation/course of pregnancy. The mice on days 3.5, 4.5, and 5.5 p.c., after in vivo gene transfer, were killed by administration of an excess of anesthetic. The uteri were removed and snap-frozen in liquid nitrogen. Day 4.5 p.c. pregnant animals received an i.v. injection of 0.5% Evans blue 15 min prior to killing to visualize the implantation sites [14]. Uteri on day 6.0 p.c. were fixed in buffered 10% formalin and stained by hematoxylin and eosin. The others were weighed every day at 21:00 and observed until their delivery.

Nuclear extract preparation and electrophoretic mobility shift assay. Nuclear proteins from uterine tissue were prepared as described previously [1]. Nuclear extract was aliquoted, snap-frozen in liquid nitrogen, and stored at −80 °C. Protein concentration was determined using a Bio-Rad protein assay kit (Bio-Rad Laboratories, CA) according to the manufacturer's instructions.

For electrophoretic mobility shift assay (EMSA), sense and antisense oligonucleotides corresponding to the κB consensus sequence [15] were synthesized by Hokkaido System Science (Sapporo, Japan), annealed, and labeled with [α-^{32}P]dCTP (Amersham Biosciences, NJ) by the Klenow fill-in reaction. Labeled probe was purified by Sephadex G-50 (Amersham) spun column fractionation. For labeled NF-κB probe, the oligonucleotides used were: sense 5′-AGTTGAGGGGA CTTTCCCAGG-3′, antisense 5′-GCCTGGGAAAGTCCCCTCAA CT-3′. For cold NF-κB probe, sense oligomer 5′- AGTTGAGGGGA CTTTCCCAGGC-3′ was annealed with the corresponding antisense oligomer. The binding reaction was performed in 20 μl with approximately 1 ng (10,000 cpm) of labeled NF-κB probe at room temperature (22 °C) for 30 min. Then the mixture was electrophoresed at 4 °C on a 5% polyacrylamide gel made with 0.5× TBE buffer [1]. To determine the binding specificity, an excess (10×–1000×-fold) of cold NF-κB probe was added 10 min before the addition of labeled NF-κB probe. EMSA was performed for nuclear extracts from five animals of each condition, and the signal intensities of shifted bands were analyzed using Fuji BAS 2500 image analyzer (Fuji Photo Film, Tokyo, Japan).

RT-PCR. Total RNA was extracted from approximately 1/4 of a uterus by using TRIZOL (Invitrogen), according to the manufacturer's instructions. Single-stranded cDNA was synthesized from 3 μg of total RNA using 50 ng of random primers (Invitrogen) and 200 U of SuperScriptII Reverse Transcriptase (Invitrogen). One-tenth of the first-strand cDNA product was subjected to PCR. PCR on complementary DNA was performed with primers purchased from Hokkaido System Science using rTaq DNA polymerase (Toyobo, Osaka, Japan). The PCR-primer sequences were: for LIF: 5′-GGAGTCCAGCCCATAAT GAAGGTC-3′ and 5′-GGCCTGGACCACCACACTTATGAC-3′ (annealing temperature: 58 °C), Hoxa-10: 5′-GTGAGTTCTGGGGC AGAGGC-3′ and 5′-AGTTCCAAAGGCGAAAATGC-3′ (annealing temperature: 68 °C), and COX-2: 5′-TTCAGGGAGAAGCGTTTGC-3′ and 5′-ACACACTCTATCACTGGCACC-3′ (annealing temperature: 60 °C). Primers for G3PDH were purchased from Toyobo. After 30 cycles of PCR (which before amplification reached a plateau), the products were subjected to electrophoresis in a 2% agarose gel and visualized by ethidium bromide staining. PCR was performed for four samples for each condition, and the mRNA levels were analyzed using the NIH image software program (http://rsb.info.nih.gov/nih-image/) and normalized against the level of G3PDH mRNA. As a negative control, the same procedure without addition of reverse transcriptase was performed for each primer set.

Statistical evaluation of results. Statistical analysis was performed using the Mann–Whitney *U* test, and differences with p value less than 0.05 were considered significant.

Results and discussion

Transient transfection of IκBαM effectively suppressed NF-κB activity in the uterus

We transfected IκBαM cDNA driven by the cytomegalovirus promoter (pcDNA3-IκBαM) into the mouse uterine cavity on day 1.5 p.c. as described previously

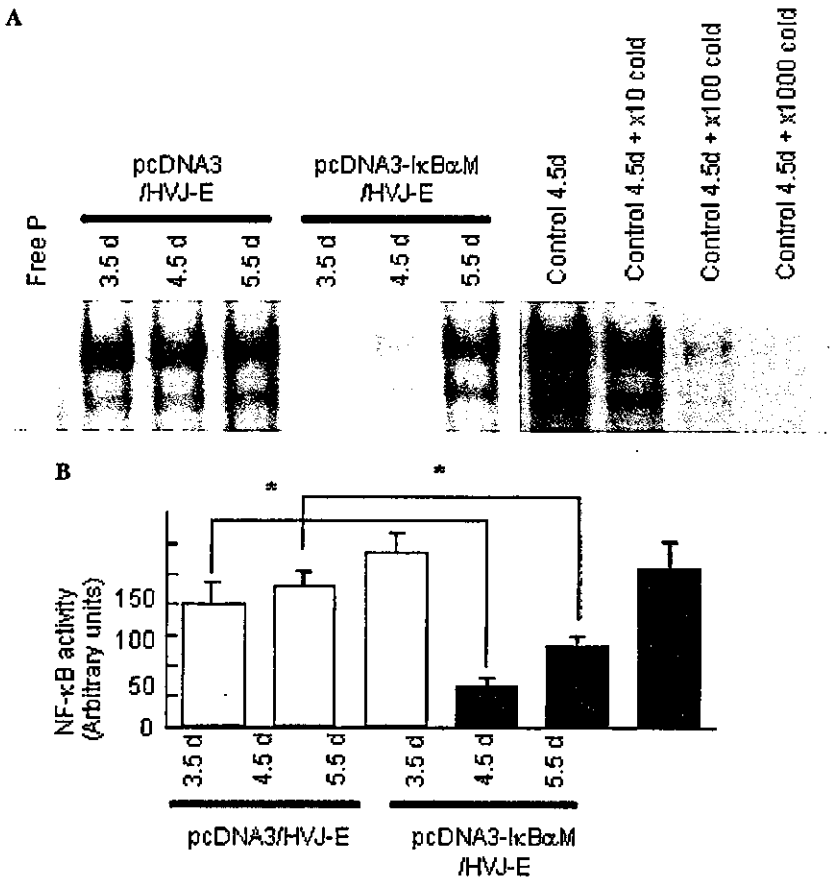

Fig. 1. NF-κB activity after in vivo gene transfer of IκBαM cDNA. Nuclear extract (5 μg) from whole uterus, obtained after pcDNA3 or pcDNA3-IκBαM-transfection at days 3.5, 4.5, and 5.5 p.c., was electrophoresed with ^{32}P-labeled κB consensus sequence probe (~10,000 cpm) in a 0.5× TBE-5% polyacrylamide gel (A). The specificity of the shifted signal was determined by addition of an excess of cold probe (10×–1000×). NF-κB activity determined as the intensity of the shifted signal was calculated and compared (B). Each group consisted of five individual mice. Asterisks indicate that p values were less than 0.05 by the Mann–Whitney U test.

[11]. By EMSAs, NF-κB activity in the nuclear extract from the whole uterus after pcDNA3-IκBαM-transfection was significantly suppressed on days 3.5 and 4.5 p.c. as compared to the control uteri (Figs. 1A and B). The specificity of the shifted signals was shown by cold inhibition experiments (Fig. 1A). The NF-κB activity was suppressed up to 72 h after IκBαM-transfection and recovered to the control level on day 5.5 p.c. (Figs. 1A and B). These results indicated that the transfection of IκBαM cDNA effectively suppressed NF-κB activity in the uterus. The total amount of IκBα was not different after pcDNA3-IκBαM-transfection, as shown by Western blotting using cytoplasmic extract of the whole uterus (data not shown). This is probably because the expression of exogenous IκBα was so localized in endometrium that the change after transfection was obscured by the large amount of endogenous IκBα protein in the whole uterus.

Effect of in vivo IκBαM transfer on the course of pregnancy

On day 4.5 p.c., implantation sites are clearly determined as blue bands in the uterus after intravenous Evans blue injection in pcDNA3-transfected mice, however few blue bands were detectable in the uterus after pcDNA3-IκBαM-transfection (Figs. 2A and B). It indicates that implantation had not occurred in the IκBαM cDNA-transfected uteri on day 4.5 p.c. On day 6.0 p.c., implantation sites are clearly visible in all of mice tested (each group $n = 5$, data not shown), however the fetuses and the uterus of the pcDNA3-IκBαM-transfected group were smaller than those of the control group (Figs. 2C and D). High-power field observation revealed that the fetus after pcDNA3 plasmid transfection had already formed an egg cylinder and posterior amniotic fold and the trophoblast layer had already invaded the endometrial stroma (Figs. 2E and G). In contrast, the embryo after pcDNA3-IκBαM-transfection had formed an epiblast and primitive endoderm (Figs. 2F and H). The development stages of these fetuses were stage 10 (equivalent to day 6.0 p.c.) and stage 6 (equivalent to day 4.0 p.c.) by Theiler [16], respectively. This difference was reproducible in 5 mice in each group on day 6.0 as well as on day 10.0 (data not shown). The course of daily maternal body weight gain indicated that the weight gain curve in the

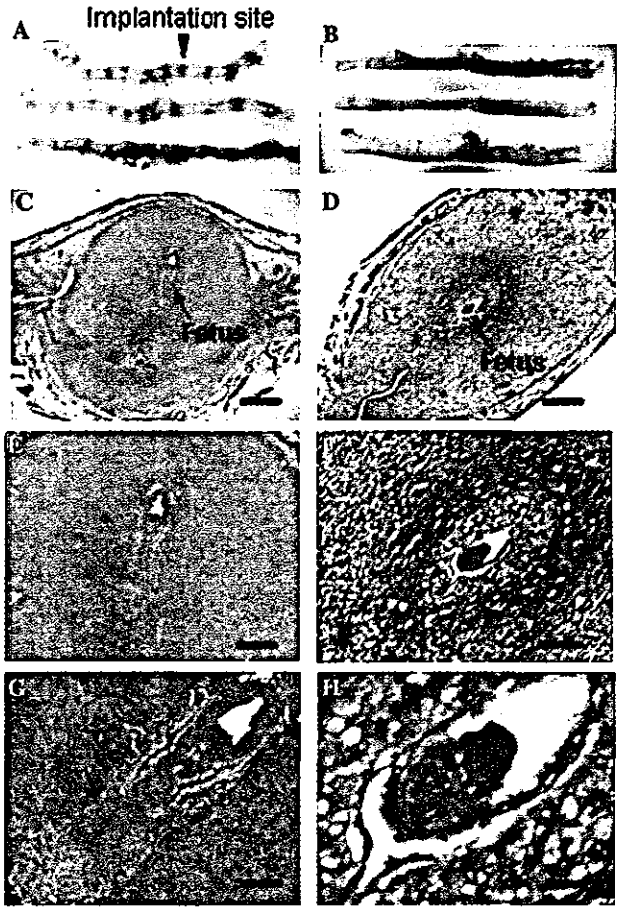

Fig. 2. Macroscopic (day 4.5 p.c.) and microscopic (day 6.0 p.c.) appearance of the uterus and fetus after IκBαM transfer. The mice were transferred IκBαM cDNA or control plasmid on day 1.5 p.c. Implantation sites were determined at day 4.5 p.c. by an i.v. injection of 0.1 ml of 0.5% Evans Blue 10 min before the mice were sacrificed. The implantation sites from pcDNA3 transferred uterus (A) were clearly detected. On the other hand, in the uterus after IκBαM cDNA transfection, implantation sites were not observed at day 4.5 p.c. (B). Hematoxylin and eosin staining of the uterus at day 6.0 p.c. (C–H). The uterus and fetuses after IκBαM cDNA transfection (D,F,H) were clearly smaller than those after transfection of pcDNA3 (C,E,G). The fetus after pcDNA3 transfection had already formed an egg cylinder, and the trophoblast layer had already invaded into the endometrial stroma (G). The fetus after IκBαM cDNA transfer had formed an epiblast and primitive inner cell mass (H). Scale bars: (C) 500 μm, (D,E) 250 μm, (F,G) 100 μm, and (H) 25 μm.

pcDNA3-IκBαM-transfected group was shifted approximately 1 day later than the curve of pcDNA3 or with sham treatment (HTF injection) (data not shown). These observations support the idea that the suppression of NF-κB activity in the uterus delayed the implantation without disturbing the course of pregnancy. Indeed, although the pregnancy rate after transfection of pcDNA3-IκBαM tended to be lower (78.6%) than the control rate, the litter size, mean birth weight, and cranio-rump length of pups were similar in both groups (Table 1). The range of litter size per mouse after pcDNA3-IκBαM transfer was wide. Although the reason is unclear, the uneven distribution of IκBαM cDNA may rarely occur and affect the implantation efficiency. Indeed, 81.8% of the mice carried 5–9 fetuses, equivalent to control mice. Only the date of parturition was significantly different, being approximately 1 day later in the pcDNA3-IκBαM-transfection group (Table 1).

Expression of LIF, HOXA-10, and COX-2 after IκBαM transfer

In the uterine endometrium at the implantation period, hundreds of genes are up-regulated and down-regulated, as revealed by microarray-based bioinformatics experiments [17–19]. On the other hand, previous gene targeting experiments clearly demonstrated the importance of LIF [20], COX-2 [21], and Hoxa-10 [22] expression at the time of implantation. We therefore tested the amount of transcripts for LIF, Hoxa-10, and COX-2 by semiquantitative RT-PCR in uterus. As shown in Fig. 3A, the levels of transcripts for Hoxa-10 and COX-2 in the whole uteri were equivalent between the both groups. The levels of LIF mRNA on days 3.5 and 4.5 p.c. were significantly lower in pcDNA3-IκBαM-transfected uteri than in control uteri (Figs. 3A and B). The gene structure of murine LIF has been characterized [23] and the regulation of this gene is very complex [24]. There is only indirect evidence that NF-κB actually regulates LIF expression [25]. We examined whether overexpression of LIF cDNA would compensate the suppression of NF-κB activity on day 4.5 p.c.

Table 1
Effect of IκBαM transfer in mouse uterus on pregnancy

	pcDNA3/HVJ-E	pcDNA3-IκBαM/HVJ-E	
Pregnancy rate (%)	100 (20/20)	78.6 (11/14)	NS
Date of delivery (day of post coitus)	19.17 ± 10.31	20.00 ± 0.22	$p < 0.05$
Range	18–20	19–21	
Litter size/mouse	7.17 ± 0.54	7.54 ± 0.96	NS
Range	5–9	1–12	
Birth weight (g)	1.68 ± 0.03	1.63 ± 0.03	NS
Range	1.27–2.14	1.19–2.02	

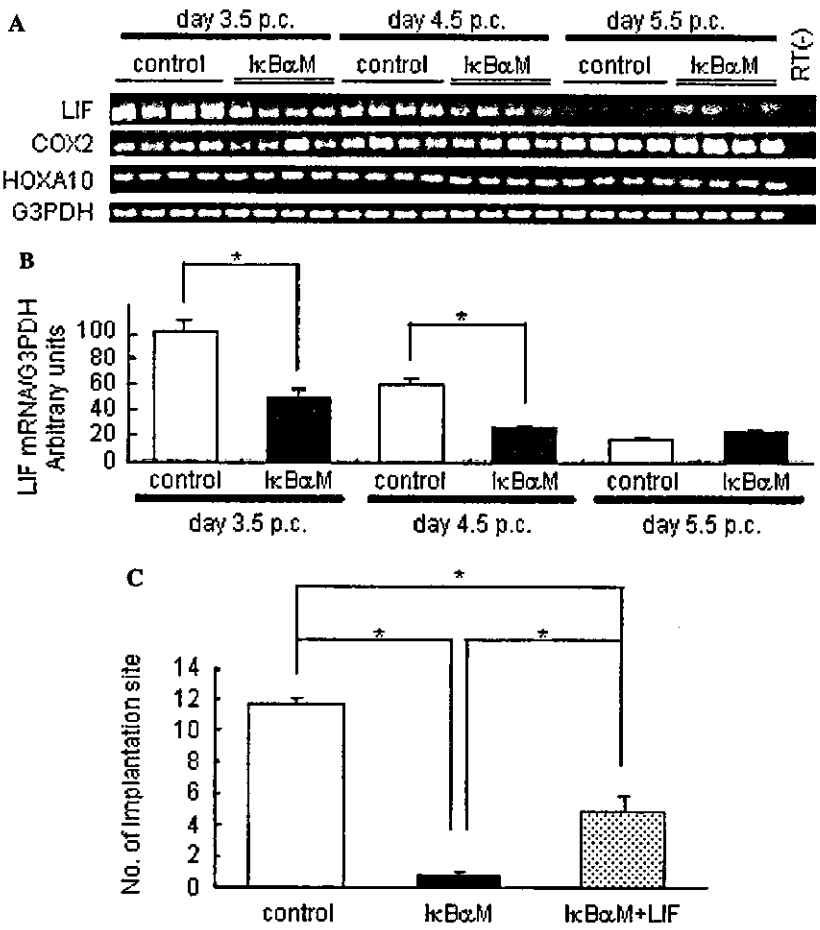

Fig. 3. Expression of LIF, COX-2, and Hoxa-10 mRNAs during the implantation period of the mouse uterus. Total RNA was prepared from the whole uterus on the indicated days under the conditions described in Materials and methods. After gel electrophoresis, RT-PCR products were visualized by ethidium bromide (A). Four animals were used for each condition. In the RT (−) lanes, the same RT-PCR procedure was performed without the addition of reverse transcriptase. The relative expression level of LIF mRNA was quantitated using NIH image (B). The signal intensities of G3PDH, amplified from the same first-strand cDNA, were used for reference. All bars represent the mean ± SEM from four animals. Asterisk indicates $p < 0.05$. The mice were transferred pcDNA3 + pcDNA3-LacZ, pcDNA3-IκBαM + pcDNA3-LacZ or pcDNA3-IκBαM + pcDNA3-LIF on day 1.5 p.c. (C). The implantation sites were detected by an i.v. injection of 0.5% Evans blue at day 4.5 p.c. The number of implantation sites in control mice ($n = 8$; 11.6 ± 0.4, range: 10–13) was significantly higher than that in pcDNA3-LacZ + pcDNA3-IκBαM ($n = 10$; 0.7 ± 0.42, range: 0–3) or pcDNA3-IκBαM + pcDNA3-mLIF ($n = 8$; 4.9 ± 0.9, range: 1–9) transfected mice. The number of implantation sites in LIF + IκBαM cDNA transferred mice was significantly higher than that in IκBαM cDNA transferred mice. Asterisk indicates $p < 0.05$.

Overexpression of LIF cDNA partially rescued delay of implantation

We transfected mouse LIF cDNA (pcDNA3-LIF) into mouse uterus simultaneous with pcDNA3-IκBαM using HVJ-E vector. As shown in Fig. 3C, significantly higher numbers of implantation sites, detected by intravenous Evans blue administration on day 4.5 p.c., were observed in pcDNA3-LIF-transfected mice than in pcDNA3-lacZ-transfected mice. However, the number of implantation sites rescued by LIF transfection was smaller than that in control (pcDNA3 + pcDNA3-lacZ transfected) mice (Fig. 3C).

The mechanism of NF-κB activation is very complicated. IκBαM is not the unique suppressor of NF-κB. A number of IκB family members, which share a common structure composed of the ankyrin repeat domain, have now been identified [15]. Another member of IκB family protein might contribute, in part, to the regulation of NF-κB activity in the mouse uterus. In vivo overexpression of mutant or native IκBα has been shown to successfully suppress pathological NF-κB activation in a mouse model. However in these models, suppression of NF-κB activity was not complete [26,27], as observed in our experiments. The level and duration of suppression of the NF-κB activity reported here appear to be relevant to altering the timing of implantation.

Our partial but significant rescue of implantation by LIF cDNA transfection suggests that LIF is one of the factors that control the timing of implantation under the regulation of NF-κB activation. Various molecules including cytokines, growth factors, and matrix

substrates regulate implantation [28] and some of them are under the regulation of cross talk between the embryo and the uterus. These molecules regulate each other in a cascade-like manner [29]. Our experimental results indicated that the activation of NF-κB is located upstream in this regulatory cascade for determination of the timing of implantation window opening. The relationship between LIF expression level in the uterus and the success of pregnancy in humans is controversial [30,31]. Discrepancy between hormonal milieu and endometrial morphology/function might be an important cause of implantation failure in human [32]. Activity of NF-κB-LIF system at the time of human implantation should be precisely characterized in these patients. This system could become a therapeutic target for implantation failure caused by discrepancy between endocrine system and endometrial function.

Acknowledgments

We thank Ms. Satomi Okamoto for technical assistance and Professor Yasuo Kiso (Yamaguchi University) for critical advice to our manuscript. This work was supported in part by Grants-in-Aid for Scientific Research (Nos. 14571557, 15390505, 15591746, and 16390476) from the Ministry of Education, Science and Culture of Japan (Tokyo, Japan).

References

[1] H. Nakamura, T. Kimura, K. Ogita, T. Nakamura, M. Takemura, K. Shimoya, S. Koyama, T. Tsujie, M. Koyama, Y. Murata, NF kappaB activation at implantation window of the mouse uterus, Am. J. Reprod. Immunol. 51 (2004) 16–21.

[2] B.C. Paria, H. Song, S.K. Dey, Implantation: molecular basis of embryo-uterine dialogue, Int. J. Dev. Biol. 45 (2001) 597–605.

[3] K. Yoshinaga, Inhibition of implantation by advancement of uterine sensitivity and refractoriness, Prog. Reprod. Biol. 7 (1980) 189–199.

[4] L.G. Giudice, Potential biochemical markers of uterine receptivity, Hum. Reprod. 14 (Suppl. 2) (1999) 3–16.

[5] G. Shyamala, M.-C. Guiot, Activation of κB-specific proteins by estradiol, Proc. Natl. Acad. Sci. USA 89 (1992) 10628–10632.

[6] M. Page, E.M. Tuckerman, T.C. Li, S.M. Laird, Expression of nuclear factor kappa B components in human endometrium, J. Reprod. Immunol. 54 (2002) 1–13.

[7] W.C. Sha, H.C. Liou, E.I. Tuomanen, D. Baltimore, Targeted disruption of the p50 subunit of NF-kappa B leads to multifocal defects in immune responses, Cell 80 (1995) 321–330.

[8] F. Weih, D. Carrasco, S.K. Durham, D.S. Barton, C.A. Rizzo, R.-P. Ryseck, S.A. Lira, R. Bravo, Multiorgan inflammation and hematopoietic abnormalities in mice with a targeted disruption of RelB, a member of the NF-κB/Rel family, Cell 80 (1995) 331–340.

[9] A.A. Beg, W.C. Sha, R.T. Bronson, S. Ghosh, D. Baltimore, Embryonic lethality and liver degeneration in mice lacking the RelA component of NFκB, Nature 376 (1995) 167–170.

[10] Q. Li, G. Estepa, S. Memet, A. Israel, I.M. Verma, Complete lack of NF-κB activity in IKK1 and IKK2 double-deficient mice: additional defect in neurulation, Genes Dev. 14 (2000) 1729–1733.

[11] H. Nakamura, T. Kimura, H. Ikegami, K. Ogita, S. Koyama, K. Shimoya, T. Tsujie, M. Koyama, Y. Kaneda, Y. Murata, Highly efficient and minimally invasive in-vivo gene transfer to the mouse uterus using haemagglutinating virus of Japan (HVJ) envelope vector, Mol. Hum. Reprod. 9 (2003) 603–609.

[12] Y. Saeki, Y. Kaneda, Protein-modified liposomes (HVJ-liposomes) for delivery of genes, oligonucleotides and proteins, in: J.E. Celis (Ed.), Cell Biology: A Laboratory Handbook, Academic Press, San Diego, 1998, pp. 123–130.

[13] Y. Kaneda, T. Nakajima, T. Nishikawa, S. Yamamoto, H. Ikegami, N. Suzuki, H. Nakamura, R. Morishita, H. Kotani, Hemagglutinating virus of Japan (HVJ) envelope vector as a versatile gene delivery system, Mol. Ther. 6 (2002) 219–226.

[14] Y.M. Huet, S.K. Dey, Role of early and late oestrogenic effects on implantation in the mouse, J. Reprod. Fertil. 81 (1987) 453–458.

[15] S. Ghosh, M.J. May, E.B. Kopp, NF-kappaB and Rel proteins; evolutionarily conserved mediators of immune responses, Annu. Rev. Immunol. 16 (1998) 225–260.

[16] K. Theiler, The House Mouse: Atlas of Embryonic Development, Springer-Verlag, New York., 1989.

[17] K. Yoshioka, F. Matsuda, K. Takakura, Y. Noda, K. Imakawa, S. Sakai, Determination of genes involved in the process of implantation: application of GeneChip to scan 6500 genes, Biochem. Biophys. Res. Commun. 272 (2000) 531–538.

[18] J. Reese, S.K. Das, B.C. Paria, H. Lim, H. Song, H. Matsumoto, K.L. Knudtson, R.N. DuBois, S.K. Dey, Global gene expression analysis to identify molecular markers of uterine receptivity and embryo implantation, J. Biol. Chem. 276 (2001) 44137–44145.

[19] L.C. Kao, S. Tulac, S. Lobo, B. Imani, J.P. Yang, A. Germeyer, K. Osteen, R.N. Taylor, B.A. Lessey, L.C. Giudice, Global gene profiling in human endometrium during the window of implantation, Endocrinology 143 (2002) 2119–2138.

[20] C.L. Stewart, P. Kaspar, L.J. Brunet, H. Bhatt, I. Gadi, F. Kontgen, S.J. Abbondanzo, Blastocyst implantation depends on maternal expression of leukemia inhibitory factor, Nature 359 (1992) 76–79.

[21] H. Lim, B.C. Paria, S.K. Das, J.E. Dinchuk, R. Langenbach, J.M. Trzaskos, S.K. Dey, Multiple female reproductive failures in cyclooxygenase 2-deficient mice, Cell 91 (1997) 197–208.

[22] I. Satokata, G. Benson, R. Maas, Sexually dimorphic sterility phenotypes in Hoxa-10-deficient mice, Nature 374 (1995) 460–463.

[23] L-W. Hsu, J.K. Heath, Identification of two elements involved in regulating expression of the murine leukaemia inhibitory factor gene, Biochem. J. 302 (1994) 103–110.

[24] B.P. Haines, R.B. Voyle, T.A. Pelton, R. Forrest, P.D. Rathjen, Complex conserved organization of the mammalian leukemia inhibitory factor gene: regulated expression of intracellular and extracellular cytokines, J. Immunol. 162 (1999) 4637–4646.

[25] S.M. Laird, E.M. Tuckerman, B.A. Cork, T.C. Li, Expression of nuclear factor kappaB in human endometrium; role in the control of interleukin 6 and leukemia inhibitory factor production, Mol. Hum. Reprod. 6 (2000) 34–40.

[26] I. Lavon, I. Goldberg, S. Amit, L. Landsman, S. Jung, B.-Z. Tsuberi, I. Barshack, J. Kopolovic, E. Galun, H. Bujard, Y. Ben-Neriah, High susceptibility to bacterial infection, but no liver dysfunction, in mice compromised for hepatocyte NF-κB activation, Nat. Med. 6 (2000) 573–577.

[27] F. Squadrito, B. Deodato, G. Squadrito, P. Seminara, M. Passaniti, F.S. Venuti, M. Giacca, L. Minutoli, E.B. Adamo, M. Bellomo, Gene transfer of IκBαlimits infarct size in a mouse model of myocardial ischemia–reperfusion injury, Lab. Invest. 83 (2003) 1097–1104.

[28] L.C. Giudice, Genes associated with embryonic attachment and implantation and the role of progesterone, J. Reprod. Med. 44 (1999) 165–171.
[29] B.C. Paria, J. Reese, S.K. Das, S.K. Day, Deciphering the cross-talk of implantation: advances and challenges, Science 296 (2002) 2185–2188.
[30] E. Hambartsoumain, Endometrial leukemia inhibitory factor (LIF) as a possible cause of unexplained infertility and multiple failures of implantation, Am. J. Reprod. Immunol. 39 (1998) 137–143.
[31] F. Olivennes, N. Ledee-Bataille, M. Samama, J. Kadoch, J.-L. Taupin, S. Dubanchet, G. Chaouat, R. Frydman, Assessment of leukemia inhibitory factor levels by uterine flushing at the time of egg retrieval does not adversely affect pregnancy rates with in vitro fertilization, Fertil. Steril. 79 (2003) 900–904.
[32] T.C. Li, L. Klentzeris, C. Barratt, M.A. Warren, S. Cooke, I.D. Cooke, A study of endometrial morphology in women who failed to conceive in a donor insemination programme, Br. J. Obstet. Gynaecol. 100 (1993) 935–938.

Available online at www.sciencedirect.com
SCIENCE DIRECT
Clinical Immunology 112 (2004) 92–105
CLINICAL IMMUNOLOGY
www.elsevier.com/locate/yclim

Hemagglutinating virus of Japan protein is efficient for induction of $CD4^+$ T-cell response by a hepatitis B core particle-based HIV vaccine

Satoshi Takeda,[a] Kouichi Shiosaki,[b] Yasufumi Kaneda,[c] Tetsuya Nakasatomi,[a] Hitomi Yoshizaki,[a] Kenji Someya,[a] Yusuke Konno,[c] Yasuyuki Eda,[b] Youichirou Kino,[b] Naoki Yamamoto,[a] and Mitsuo Honda[a,*]

[a] *AIDS Research Center, National Institute of Infectious Diseases, Tokyo 162-8640, Japan*
[b] *The Chemo-Sero-Therapeutic Research Institute, Kumamoto 869-1298, Japan*
[c] *Division of Gene Therapy Science, Osaka University School of Medicine, Osaka 565-0871, Japan*

Received 10 June 2003; accepted with revision 5 April 2004

Abstract

By using the hepatitis B core (HBc) protein gene as a carrier, HIV-1 *env V3* gene was inserted into the carrier gene, and the HIV gene was expressed inside a chimeric HIV-HBc particle (HIV-HBc), which was a unique candidate for induction of HIV-specific CTL activity. This was seen significantly in mice without the need of an adjuvant, because other responses specific for the HIV peptide such as T-cell proliferation and antibody production were not induced. However, when hemagglutinating virus of Japan (HVJ) protein was incorporated into an anionic liposome containing HIV peptide (HIV-HVJ-liposome) and was used as a booster immunization in HIV-HBc primed animals, the HIV-specific T-cell response and enhanced CTL activity were clearly induced in consecutively immunized animals. Furthermore, the HIV-specific humoral immune response was also induced and a neutralization activity was detected in the immune sera. Thus, when an HIV peptide antigen is expressed inside the virus like a particle of HBc, it can induce both cellular and humoral immunities when an HVJ-HIV-liposome, but not an HIV-liposome, is inoculated as the booster antigen. The *HVJ*-stimulated splenocytes secreted *IL*-18 and IL-12 to synergistically enhance the secretion of IFN-γ in vitro. These findings suggest that the HVJ protein is effective at inducing the HIV-specific immunities, if used as part of a booster antigen in the consecutive immunization regimen.

Keywords: HVJ protein-incorporated liposome; HIV-hepatitis B core chimeric protein; HIV-specific immunity; Synergy of IL-18 and -12 to secrete IFN-γ

Introduction

A variety of novel approaches are currently being investigated to promote effective immunity against HIV-1. Such approaches often include attenuated, recombinant bacterial vectors that express antigenic epitopes from those of HIV [1–4], recombinant adenovirus vectors [5], recombinant vaccinia virus [6], DNA vaccines expressing gp120 [7], and synthetic peptides containing T- and B-cell epitopes of HIV as immunogens [8,9]. These candidate vaccines rely on the induction of both cellular and humoral immunities. It has been suggested that such immunities help protect individuals from HIV infection and from the subsequent development of AIDS [10]. Furthermore, HIV-specific $CD4^+$ T-cell response may play a critical role in vaccine development and immunother-

Abbreviations: HVJ, hemagglutinating virus of Japan; HBc, hepatitis B core protein; HIV-HBc, chimeric HIV-V3-HBc particle; HVJ-liposome, liposome with incorporated HVJ protein; HIV-liposome, liposome which encapsulated circular HIV-V3 peptide; HIV-HVJ-liposome, HVJ-liposome which encapsulated HIV-V3 circular peptide; HIV_{HXB2}-HVJ-liposome, HVJ-liposome encapsulated circular $HIV\text{-}1_{HXB2}$ V3 peptide; V3, principal neutralizing determinant; *KLH*, keyhole limpet hemocyanin; KLH-IIIB, KLH-conjugated $HIV\text{-}1_{HXB2}$ V3 peptide; BSA-IIIB, BSA-conjugated $HIV\text{-}1_{HXB2}$ V3 peptide; Chol, Cholesterol; PC, phosphatidylcholine; Sph, shingomyelin; DOPE, dioleoylphosphatidylethanolamine; DC-chol, dimethylaminoethane carbamoyl-cholesterol; HAU, hemagglutinating unit; SI, stimulation index.

* Corresponding author. AIDS Research Center, National Institute of Infectious Diseases, 1-23-1 Toyama, Shinjuku-ku, Tokyo 162-8640, Japan. Fax: +81-3-5285-1183.
E-mail address: mhonda@nih.go.jp (M. Honda).

1521-6616/$ - see front matter © 2004 Elsevier Inc. All rights reserved.
doi:10.1016/j.clim.2004.04.001

apeutic interventions that aim to maintain effective immunity to HIV infection [11].

To render subunits of viral antigen or synthetic peptides immunogenic, a T helper cell's peptide or protein is fused to a target peptide [8,12], because free synthetic peptides or proteins are usually poor immunogens. For several reasons, the hepatitis B core (HBc) protein is a potential target carrier peptide [13–17]: (i) HBc can be assembled and can form particles that can induce immunity without the use of an adjuvant [18]. (ii) HBc Ag is a strong T-cell immunogen and is recognized over a wide range of MHC haplotypes [19]. (iii) The HBc Ag gene has been fused with respective target epitope genes to the N terminus [20–24], to the C terminus [14], and to internal sites [16,23,25,26]. In the present study, the HIV gene was inserted at the internal site of the HBc gene and the antigen was expressed inside the particles of the HBc chimeric protein (HIV-HBc) that spontaneously aggregated to a rigid particle of approximately 30 nm in diameter. This type of antigen inside the particle induced antigen-specific CTL but could not induce the antigen-specific $CD4^+$ T-cell response. These findings suggest that the HIV-HBc antigen may not be a suitable immunogen when used alone. However, the HIV-specific T-cell response is effectively inducible when the hemagglutinating virus of Japan (HVJ) protein was incorporated into anionic-type HIV-liposomes encapsulated by circular HIV-V3 peptides (HIV-HVJ-liposome). The HIV-HVJ-liposome was used as a booster injection in HIV-HBc primed animals.

In this paper, we chose the third variable domain (V3) of HIV-1 isolates' gp120 as an immunogen, because it evokes neutralizing antibody recognizing V3-tip region with a low efficiency by itself [27]. The V3 region is suggested to be immunodominant and so of importance in vaccine development [28]. The site is also assumed to be a chemokine receptor-binding site by the crystal structure analysis [29–31]. Furthermore, strong cellular immune responses and high HIV-specific neutralizing activity may account for long-term nonprogression in different individuals [32,33]. To improve immunogenicity of the V3 site for immunization of experimental animals, we designed to enhance immune induction of the HIV V3-specific immunity by using the HVJ protein-incorporated anionic liposome.

Materials and methods

Animals

Female eight-week-old BALB/c mice ($H\text{-}2^d$), and 6-week-old Hartley strain guinea pigs (400 g), were purchased from the Japan SLC Co., Ltd., Hamamatsu, Japan and were used within 10 days. All animal care and housing requirements determined by the National Institute of Infectious Diseases (NIID) committee for the care and use of laboratory animals were followed. Animal protocols were reviewed and approved by an institutional animal care and use committee.

Construction of expression vectors and preparation of HIV-HBc chimeric particles

A synthetic DNA fragment encoding 21-aa or 19-aa V3 tip sequence of $HIV\text{-}1_{HXB2}$ or $HIV\text{-}1_{MN}$, respectively, was inserted into plasmid pYGHBc [34], which are seen in yeast cells. The product of HIV-HBc chimeric particles were purified and prepared as a vaccine antigen by using the methods described by Shiosaki et al. [15] and Miyanohara et al. [18]; however, different oligonucleotides were used for the present study. The monoclonal antibodies used for the antigen analysis by ELISA, Western immunoblot, and immuno-electron microscopy, were anti-HBc antibody [18], anti-HIV_{HXB2} V3 mAb 0.5β [35], and anti-HIV_{MN} V3 mAb μ5.5 [36].

Preparation of both anionic and cationic HIV-HVJ-liposomes

Lipids

Cholesterol (Chol), egg yolk phosphatidylcholine (PC), and egg yolk sphingomyelin (Sph) were purchased from Sigma (St. Louis, MO). Bovine brain phosphatidylserine (PS) was purchased from Avanti Polar Lipids Inc. (Birmingham, AL). Dioleoylphosphatidylethanolamine (DOPE) and dimethylaminoethane carbamoyl-cholesterol (DC-chol) were obtained from NOF Corporation (Tsukuba, Ibaraki, Japan).

Preparation of HVJ

HVJ (Z strain) was grown in chorioallantoic fluid of 10-day-old embryonated chicken eggs at 36.5 °C. HVJ was collected as a pellet by centrifugation at 27,000 × *g* for 30 min at 4 °C and was suspended with a balanced salt solution (BSS; 10 mM Tris–HCl pH 7.5, 137 mM NaCl, 5.4 mM KCl). RNA genome of HVJ was inactivated by UV irradiation (198 mJ/cm^2) just before use.

Preparation of anionic-type and cationic-type liposomes

First, lipid mixtures were prepared by dissolving PC (1.63 mg), DOPE (1.53 mg), Sph (1.47 mg), and Chol (3 mg) in 0.5 ml chloroform. PS (1.25 mg) or DC-chol (0.75 mg) was added to the lipid mixtures to prepare the anionic-type or cationic-type HVJ-liposomes, respectively. The lipids in chloroform was transferred to a glass tube and dried as a thin lipid film by evaporation, as described elsewhere [37]. Both of the HIV Env V3 synthetic circular peptides; circular IIIB-V3, VEINCTRPLNNTRKSIRIQRGPGRAFVTIGSIIGDIRQAHCNLSR; and circular MN-V3, VEINCTRPNNNTRKSIHIGPGRAFYTTGSIIGDIRQAHCNLSR (1.67 mg each, Takara Shuzo Co., Ltd., Kusatsu, Shiga, Japan) were dissolved in 200 μl of distilled water. The suspension was then added to the dried lipid mixture. Liposomes were prepared by vigorous shaking, as described previously [38]. In the case of the anionic-type liposomes, they were sonicated for 3 s and 300 μl of BSS

was added to the liposomes followed by gentle shaking at 37 °C for 30 min. For cationic-type HVJ-liposomes, the liposome suspension was extruded through cellulose acetate membrane filters (pore size 0.45 μm and 0.20 μm) as described previously [39].

Preparation of HVJ-liposomes

The liposome suspension prepared above was mixed with a UV-inactivated HVJ suspension [15,000 hemagglutinating unit (HAU)] for 10 min on ice and incubated at 37 °C for 1 h while shaking the suspension in a water bath. The HVJ-liposome complexes were then separated from free HVJ by sucrose density gradient centrifugation (62,800 × *g* at 4 °C for 1.5 h). The HVJ-liposomes between BSS and 30% sucrose solution were collected. The volume of HVJ-cationic liposome was adjusted to 300 μl with BSS. The HVJ-anionic liposomes were diluted 4 times with BSS and centrifuged at 27,000 × *g* for 30 min at 4 °C. The pellets were suspended with 300 μl of BSS by vortexing.

Enzyme-linked immunosorbent assay

Peptide-based ELISA, as described previously [40], was performed to detect antigen-specific antibodies within the guinea pig.

Cytotoxicity assays

The procedure for in vitro CTL activation and in vitro effector cell assay has been described previously [28,41–43]. In brief, spleen cells were isolated from mice immunized with vaccine antigens. Primed and washed cells (1×10^7) were incubated for 6 days with 10 μg of synthetic V3 peptide per milliliter. The restimulated spleen cells were incubated for 4 h with ^{51}Cr-labeled M12.4.5 (H-2^d), BW5147 (H-2^k), and S49 (H-2^s) cell lines used as target cells. The target cells were treated with ^{51}Cr at a concentration of 100 μCi for 90 min, and were then pulsed with 10 μg of the synthetic V3 peptide for 60 min. The BW5147 (H-2^k) and S49 (H-2^s) cell lines were kindly provided by Dr. Ethan M. Shevach, National Institutes of Health, Bethesda, MD; these cells were also used as target cells. The percentage of specific release was calculated as follows: % specific release = [(experimental release − spontaneous release)/(maximum release − spontaneous release)] × 100. The sequences of synthetic peptides of HIV_{HXB2} and HIV_{MN} V3 region of envelop proteins used for effector cells induction were RIQRGPGRAFVTIGK (P18IIIB) [42] and RIHIGPGRAFYTTKN (P18MN) [42], respectively (Takara Shuzou).

T-cell proliferation assay

Lymphocyte proliferative assays were performed as previously described [44]. Briefly, isolated spleen cells were pooled and the $CD4^+$ or $CD8^+$ fraction was then depleted using magnetic cell sorting (MACS, Militenyi Biotec., Bergisch Gladbach, Germany) [40]. Results are expressed as the stimulation index (SI), which was calculated as a ratio of the counts per minute (cpm) in the presence and absence of an antigen.

PBMC-based virus neutralization assay of HIV-1

The serum antibody of the guinea pigs inoculated with HIV-HBc following a booster injection of HIV-HVJ-liposome or a booster injection of HIV-liposome was purified from the whole sera from 15 immunized guinea pigs with Protein A Sepharose (Amersham Pharmacia Biotech, AB, Uppsala, Sweden). Serum IgG from guinea pigs injected with the HIV-HVJ-liposome and normal guinea pig IgG were also purified by the same method. The diluted serum antibodies were incubated with 100 $TCID_{50}$ units of HIV-1_{LAI}, HIV-1_{MN} and HIV-1_{Th22} (AIDS Research and Reference Reagent Program, NIH, Rockville, MD). The mixtures were incubated with PHA-activated peripheral blood mononuclear cell (PBMC). After being washed three times with PBS, the cells were cultured in the presence of recombinant human IL-2 (40 units/ml, Shionogi and Co., Ltd., Osaka, Japan) for 7 days. The amount of HIV in the supernatant was measured by HIV-1 p24 antigen ELISA (Dinabot, Ltd., Tokyo, Japan) [43,45]. The in vitro neutralization activity of the immune IgG against HIV-1 was determined by using 100 $TCID_{50}$ of the stock virus [43] and was expressed as percentage inhibition of p24 antigen production in the culture supernatants compared with that of the cultures to which serum IgG from normal guinea pigs was added. For the neutralization assays, virus stocks were titrated on PHA-activated normal PBMC and the $TCID_{50}$ of each virus was determined [43,46].

Cytokine ELISAs

Specific ELISAs determined the amounts of IL-12, IL-18, and IFN-γ in culture supernatants. IL-18 ELISA kit was purchased from Fujisaki Institute, Hayashibara Biochemical Laboratories, Okayama, Japan and IL-12 and IFN-γ ELISAs from R&D Systems Inc., Minneapolis, MN.

Statistical analysis

Calculations of the geometric mean ± SD were carried out with a microcomputer. Significance was defined as $P < 0.05$.

Results

Construction of pYGHBc-HIV and preparation of HIV-HBc chimeric particles

Each V3 peptide gene from HIV-1_{HXB2} or HIV-1_{MN} was inserted into an internal position of pYGHBc (pYGHBc-

HIV) and the amino acid sequences of the V3 regions of HIV-1_{HXB2} and HIV-1_{MN} genes were as follows (name, sequence): synthetic IIIB-V3 peptide, LNNTRKSIRIQRGP-GRAFVTI; and synthetic MN-V3 peptide, PNNKRKR IHIGPGRAFYTT (Fig. 1A). Protein particles were prepared by purification from the extract of yeast cells that expressed the pYGHBc-HIV V3 as described by Shiosaki et al. [15] and Miyanohara et al. [18] to be a single protein band (upper panel of Fig. 1B). To determine the antigen capability of the purified protein particle, we analyzed whether the purified protein particle was the fusion protein of HBc and V3 peptide of HIV-1_{HXB2} by Western blot assay (lower left panel of Fig. 1B). The protein showed reactive behavior with both anti-V3 0.5β mAb and anti-HBc Yc-3 mAb (lower left and lower right panels of Fig. 1B, respectively), indicating that the protein is a chimeric protein, which is composed of HBc protein and HIV Env V3 peptide antigen of HIV-1_{HXB2}. HIV_{MN}-HBc chimeric particle was similarly prepared.

Furthermore, the HIV-HBc chimeric proteins spontaneously aggregated to form a rigid particle of approximately 30 nm in diameter. This was seen by electron microscopy and sucrose-density ultracentrifugation analysis, and was stable at 4 °C for 2 months (data not shown). The binding

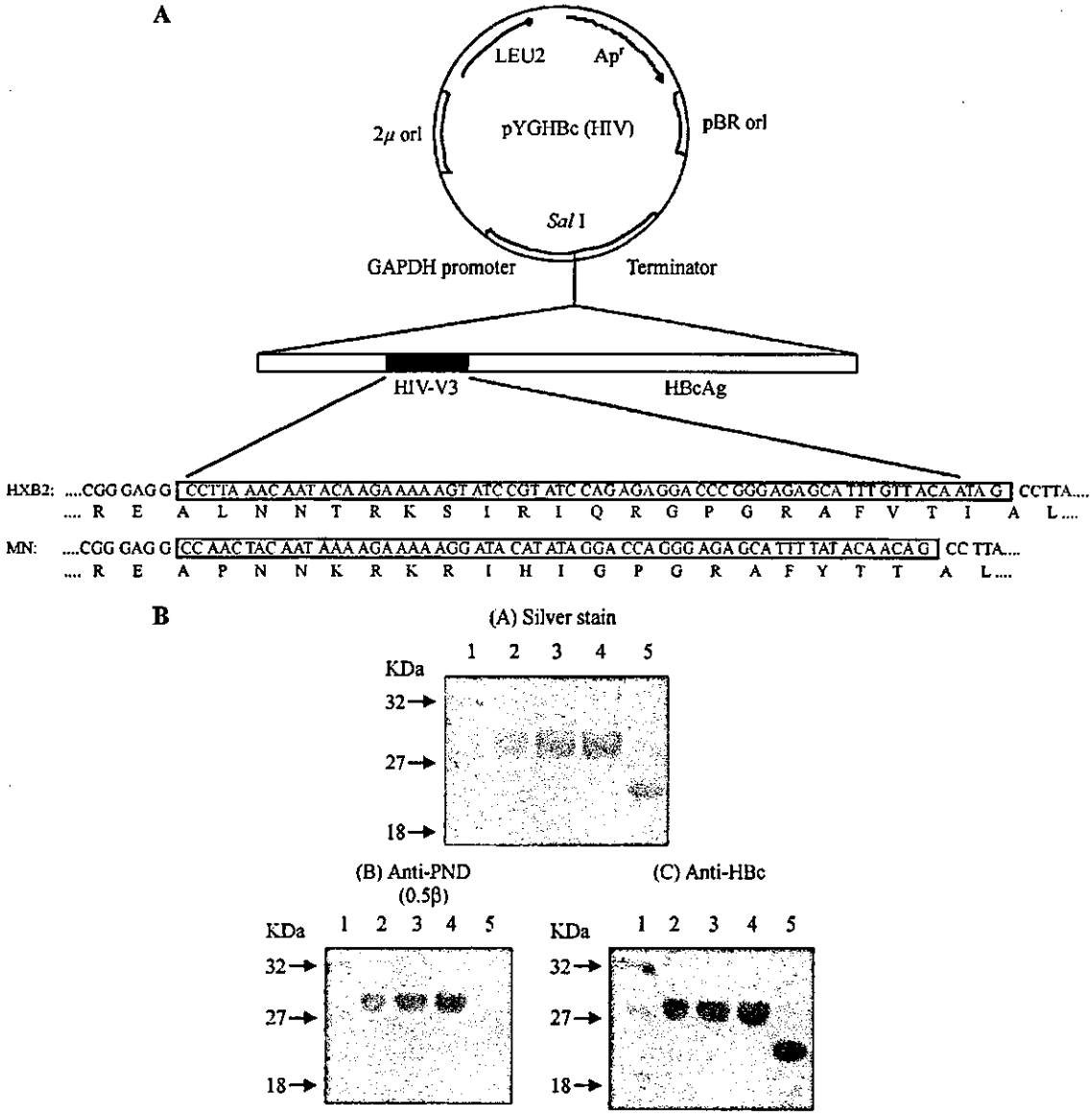

Fig. 1. Vector construction and expression of the HIV-HBc chimeric protein. (A) Vector construction of the HIV-HBc chimeric protein. DNA fragments encoding the V3-tip of the HIV V3 region from HIV-1_{HXB2}, and HIV-1_{MN} were inserted into the *Sal*I restriction site in the gene for HBc antigen in plasmid pYGHBc. Apr, pBR ori, GAPDH promoter, 2μ ori, and LEU indicate genes for resistance to the drug marker, promoter, and initiation sites. DNA sequences of inserted fragments are in boxes and their deduced amino acid sequences are aligned. (B) Detection of the HIV-HBc chimeric protein by SDS-PAGE (upper panel) and Western blotting. A purified chimeric particle was separated by SDS-PAGE and detected by Western blotting with an anti-HIV Env V3 0.5β mAb or an anti-HBc Yc-3 antibody (lower left and lower right panels). Lane 1, molecular weight marker; lanes 2–4, HIV-HBc chimeric protein; lane 5, HBc protein.

ability of the HIV-HBc chimeric particle with anti-HIV_{HXB2} V3 mAb 0.5β, and anti-HIV_{MN} V3 mAb μ5.5 was examined using the ELISA antigen and immuno-electron microscopy, resulting in that the bindings were negative for anti-V3 antibodies, in contrast the binding was positive for anti-HBc antibody (data not shown). Thus, these data suggested that the HIV peptide antigens were assumed to be inside the HIV-HBc chimeric particle but not on the surface of the particle.

Experimental protocol

As shown in Fig. 2, in the first series of experiments, mice were intradermally injected in the neck with 10 μg of HIV-HBc chimeric protein within 100 μl of saline solution. The mice were given identical booster injections s.c. 7 days later. In the next series of experiments, we determined whether booster injections of the HIV-HVJ-liposome were able to elicit or enhance both cell-mediated and humoral immunity against the HIV antigen in mice and guinea pigs. Mice were immunized twice with 10 μg of HIV-HBc in saline. Two weeks later after the second immunization, the immunized animals were given an HIV-HVJ-liposome that included 10 μg of circular HIV-V3 peptides. Guinea pigs were immunized (50 μg per animal) with the HIV-HBc in saline and followed by an administration with the HVJ-liposome that included 10 μg of HIV-V3 circular peptides. As controls, the HIV-HBc-immunized animals were boosted with liposomes that had not incorporated HVJ protein but which did include 10 μg of circular HIV-V3 peptides (HIV-liposome); HBc-immunized animals were boosted with HIV-HVJ-liposome with 10 μg of circular HIV-V3 peptides. Normal animals were also injected with the HIV-HVJ-

A. Mouse experiment

(Group)	Week 0	1	2
1.	HIV-HBc (10μg S.C.)	HIV-HBc	
2.	HBc (10μg S.C.)	HBc	

(Group)	Week 0	1	2	3	4
1.	HIV-HBc (10μg S.C.)	HIV-HBc		HIV-HVJ-liposome (10μg S.C.)	
2.	HIV-HBc (10μg S.C.)	HIV-HBc		HIV-liposome (10μg S.C.)	
3.	NBc (10μg S.C.)	HBc		HIV-HVJ-liposom (10μg S.C.)	
4.	HBc (10μg S.C.)	HBc		HIV-liposome (10μg S.C.)	
5.	HIV peptide (10μg S.C.)	HIV peptide		HIV-HVJ-liposome (10μg S.C.)	
6.	HIV peptide (10μg S.C.)	HIV peptide		HIV-liposome (10μg S.C.)	
7.	HIV-HVJ-liposome (10μg S.C.)	HIV-HVJ-liposome		HIV-HVJ-liposome	

B. Guinea-pig experiment

(Group)	Week 0	2	6	10
1.	HIV-HBc (50μg S.C.)	HIV-HBc	HIV-HVJ-liposome (10μg S.C.)	
2.	HIV-HBc (50μg S.C.)	HIV-HBc	HIV-liposome (10μg S.C.)	
3.	HBc (50μg S.C.)	HBc	HIV-HVJ-liposome (10μg S.C.)	
4.	HIV-HVJ-liposome (10μg S.C.)	HIV-HVJ-liposome	HIV-HVJ-liposome	

Fig. 2. Immunization schedule for induction of HIV-specific immunity.